

**Structural Insights into Oligomeric Protein Complexes by Electron Spin Resonance**

by

**Katherine M. Stone**

Bachelor of Science, University of Georgia, 2001

Submitted to the Graduate Faculty of  
Arts and Sciences in partial fulfillment  
of the requirements for the degree of  
Doctor of Philosophy

University of Pittsburgh

2009

UNIVERSITY OF PITTSBURGH  
FACULTY OF ARTS AND SCIENCES

This dissertation was presented

by

Katherine M. Stone

It was defended on

March 26, 2009

and approved by

Michael Cascio, Ph. D., Assistant Professor, Department of Microbiology and Molecular  
Genetics, School of Medicine

David Waldeck, Ph. D., Professor, Department of Chemistry, Faculty of Arts and Sciences

Stephen Weber, Ph. D., Professor, Department of Chemistry, Faculty of Arts and Sciences

Dissertation Advisor: Sunil Saxena, Associate Professor, Department of Chemistry, Faculty  
of Arts and Sciences

Copyright © by Katherine M. Stone

2009

# **Structural Insights into Oligomeric Protein Complexes by Electron Spin Resonance**

Katherine M. Stone, PhD

University of Pittsburgh, 2009

This thesis describes the use of site-directed spin labeling (SDSL) and electron spin resonance (ESR) for measuring distance constraints in oligomeric protein complexes. We demonstrate the use of ESR for biological systems that suffer from a lack of structural data by other methods. First, we show that distance measurements of several mutants of the EcoRI restriction endonuclease could be used to investigate the disorder to order transition. The double electron-electron resonance (DEER) ESR experiment was performed on spin labeled residues of EcoRI bound to several different sequences of DNA. We chose residues that would probe the inner and outer arms of EcoRI, which are known to play a critical role in modulating the specificity of the endonuclease. Distance measurements revealed that the average distance of each mutant remains the same when the protein is bound to different sequences of DNA. This data suggests that although EcoRI exhibits a significantly lower binding affinity to sequences of DNA differing from the specific complex, the overall structure of the arms is preserved.

SDSL and ESR were also performed on the human  $\alpha 1$  glycine receptor (GlyR), an integral membrane protein that is a member of the ligand-gated ion channel superfamily (LGICS). Seven cysteine mutants of the homopentameric complex were cloned, expressed, purified, reconstituted and spin labeled. These point mutations are located in the third transmembrane domain of GlyR and are putatively buried in the lipid bilayer. We show that the cysteines are accessible to the thiol-reactive spin label even when the channel is reconstituted in

a lipid bilayer. Using DEER-ESR, we measured the average number of coupled spins per receptor and found that for each mutant, between one and two cysteines were labeled with the spin label. The inter-spin distances were measured in each mutant. Preliminary results indicate that two distances could be distinguished, which is consistent with the pentagonal symmetry of the channel. These results establish the applicability of SDSL and ESR distance measurements for the LGICS. Such distance measurements will likely be essential for determining subunit packings and providing structural details in this important class of proteins.

## TABLE OF CONTENTS

<b>PREFACE.....</b>	<b>XIII</b>
<b>1.0 INTRODUCTION .....</b>	<b>1</b>
<b>1.1 ABSRACT.....</b>	<b>1</b>
<b>1.2 SITE-DIRECTED SPIN LABELING FOR ESR .....</b>	<b>2</b>
<b>1.3 DETERMINATION OF STRUCTURE AND DYNAMICS BY SDSL ESR.....</b>	<b>5</b>
<b>1.4 DEER-ESR.....</b>	<b>8</b>
<b>1.5 SPIN COUNTING BY DEER-ESR .....</b>	<b>16</b>
<b>2.0 ELECTRON SPIN RESONANCE SHOWS COMMON STRUCTURAL FEATURES FOR DIFFERENT CLASSES OF ECO-RI-DNA COMPLEXES .....</b>	<b>20</b>
<b>2.1 ABSTRACT .....</b>	<b>20</b>
<b>2.2 INTRODUCTION .....</b>	<b>21</b>
<b>2.3 METHODS .....</b>	<b>22</b>
<b>2.4 RESULTS AND DISCUSSION.....</b>	<b>27</b>
<b>3.0 MEASUREMENT OF INTER-SUBUNIT SEPARATIONS IN THE M3 DOMAIN OF A LIGAND GATED ION CHANNEL BY ELECTRON SPIN RESONANCE.....</b>	<b>45</b>
<b>3.1 ABSTRACT .....</b>	<b>45</b>
<b>3.2 INTRODUCTION .....</b>	<b>46</b>
<b>3.3 MATERIALS AND METHODS.....</b>	<b>52</b>

<b>3.4 RESULTS AND DISCUSSION.....</b>	<b>56</b>
<b>APPENDIX A .....</b>	<b>65</b>
<b>APPENDIX B .....</b>	<b>72</b>
<b>BIBLIOGRAPHY .....</b>	<b>76</b>

## LIST OF TABLES

Table 2.1. EcoRI equilibrium binding data to the specific site in 0.22M KCl, 20 mM Cacodylate, pH 7.3, at 21°C. $\Delta\Delta G_{\text{bind}} = -RT \ln(K_{A,\text{mut}}/K_{A,\text{wt}})$ . The second wild-type sample was subjected to a mock spin-labeling reaction lacking the spin label reagent. ....	31
Table 2.2. For each sample, the resonator used and the $P_b$ for a given length of the pump pulse is given. *The $P_b$ values were determined by S. Pornsuwan and are reported in S. Pornsuwan, PhD thesis, University of Pittsburgh (Pittsburgh), 2007. ....	36

## LIST OF FIGURES

Figure 1.1 Site-directed spin labeling of a protein. A. Methanethiosulfonate, MTSSL attaches to the free cysteine of the protein. A disulfide bond is formed. B. Structure of MTSSL.....	4
Figure 1.2 (A) Site-directed mutagenesis in tandem with site-directed spin labeling allows for the selective attachment of an ESR active label to virtually any position in the protein sequence. (B) The CW lineshape is sensitive to the local environment of the spin label, and can be used to assess the extent of tertiary interaction, as well as other structural and dynamical information. (C) The distance between two spin labels, up to $\sim 70 \text{ \AA}$ , can be measured using pulsed ESR distance methods.....	6
Figure 1.3 Energy level diagram for nitroxides. In the presence of the external magnetic field, the degeneracy of the energy levels for the spins is broken. These states are further split by the nuclear spin as $2I + 1$ .....	9
Figure 1.4. The dipolar interaction. (A) Two nitroxides in a magnetic field. Electron spins from two nitroxides are labeled 1 and 2. (B) Pake pattern showing the frequency of the dipolar interaction. ....	11
Figure 1.5 (A) Pulse sequence for the 4-pulse DEER experiment. (B) Excitation profile of the pump and observe pulses. (C) Examples of intramolecular (solid lines) and intermolecular (dotted line) interactions in a sample of doubly labeled peptides.....	12

Figure 1.6. Dependence of  $V_{\text{intra}}$  on the number of coupled spins. As doubly labeled peptide aggregates are diluted with unlabeled peptides, the modulation depth decreases and  $V_p$  increases. Figure taken from reference 49. .... 19

Figure 2.1 Excitation profile of the pump and observe frequencies shown for the R131C complexes. All DEER-ESR experiments for the R131C DNA complexes were performed with the observer frequency placed at the maximum of the nitroxide spectrum, as shown here. For the S180C and K249C-S180C complexes, the pump frequency was placed at the maximum of the nitroxide spectrum, and the observer frequency was placed at the center of the low-field component..... 25

Figure 2.2 X-ray structure of the EcoRI specific complex. A) The bottom view shows monomers in red and blue. B) The side view illustrates the arm domain by circles. The DNA sequence is shown in yellow, and the residues mutated to cysteine are highlighted in green. Coordinates are from a highly refined version <sup>[6,7]</sup> of PDB entry 1CKQ. .... 29

Figure 2.3 A field swept echo detected experiment was used to estimate the labeling efficiency of the WT EcoRI specific complex (green). Compared to the signal for the R131C NS complex (blue), which had ~100% labeling efficiency, we estimate <10% of the cysteines at position 218 were modified with MTSSL. .... 30

Figure 2.4 Unprocessed time domain DEER signal for the R131C EcoRI complexes. The dotted red line in the time domain is the background correction. .... 33

Figure 2.5 Unprocessed time domain DEER signal for the K249C-S180C EcoRI complexes. The dotted red line is the background correction..... 34

Figure 2.6 Unprocessed time domain DEER signal for the S180C EcoRI complexes. The dotted red line is the background correction, and the green line indicates the zero time. .... 35

Figure 2.7 (a) DEER data for R131C specific, miscognate and non-specific complexes. Simulated traces based on the distance distributions are overlaid on the experimental signal. (b) Normalized distance distribution functions. Red lines in the crystal structure indicate distance measured.....	39
Figure 2.8 The time domain signal for the R131C specific complex with the simulated signal overlaid in red (a) and the resulting distance distribution function (b). Time domain signal and simulated signal overlaid in green (c) for the suppression of the 55 Å peak in the distance distribution function (d).....	40
Figure 2.9 (a) DEER data for S180C specific and non-specific complexes. Simulated traces based on the distance distributions are overlaid on the experimental signal. (b) Normalized distance distribution functions. Red lines in the crystal structure indicate distance measured. ..	41
Figure 2.10 (a) DEER data for the double mutant, K249C-S180C specific, miscognate and non-specific complexes. Simulated traces based on the distance distributions are overlaid on the experimental signal. (b) Normalized distance distribution functions. Red lines in the crystal structure indicate distance measured.....	42
Figure 3.1 (a) The structure of the $\alpha$ 1 subunit of GlyR is illustrated. Each subunit consists of extracellular domain, a transmembrane domain and an intracellular loop. The star indicates the third transmembrane segment, M3. (b) Five subunits oligomerize to form a central channel through the membrane in the 250 kDa GlyR (c) Due to the pentagonal symmetry of the channel, spin labeled single cysteine mutants of GlyR yields five spin labeled positions and two unique distances, $r_1$ and $r_2$ . .....	50
Figure 3.2 (a) Unprocessed time domain DEER signal for C286-C289 mutants. The red line was used to divide out the contribution from the intermolecular interaction. (b) The background	

corrected  $V_{\text{intra}}$  DEER signal. The limiting  $V_{\text{intra}}$  value,  $V_p$  is given for each mutant as well as the number of coupled spins,  $N$ . ..... 58

Figure 3.3 (a) Unprocessed time domain DEER signal for C290-C292 mutants. The red line was used to divide out the contribution from the intermolecular interaction. (b) The background corrected  $V_{\text{intra}}$  DEER signal. The limiting  $V_{\text{intra}}$  value,  $V_p$  is given for each mutant as well as the number of coupled spins,  $N$ . ..... 59

Figure 3.4. a) The DEER-ESR time and b) frequency domain signals for GlyR mutants C286-C292. Simulated traces based on the c) distance distribution functions generated in DEERAnalysis2006 are overlaid in red. Two distances were measured for each sample averaging approximately 25 and 36 Å..... 61

Figure A.1. Flow chart for creating mutant GlyR protein. a) The gene for GlyR is mutated to code for a single free cysteine at the desired location using site-directed mutagenesis. b) The mutant GlyR gene is incorporated into bacmid DNA, and virus is created and amplified. c) The baculovirus is used to infect Sf9 insect cells and overexpress mutant GlyR protein. .... 66

Figure A.2. Site-directed mutagenesis of the GlyR. .... 68

## PREFACE

During my time at the University of Pittsburgh, there are many people who have positively contributed to my graduate career. First, I thank my research advisor, Professor Sunil Saxena. It has been an amazing opportunity to be among the first group members, and it is from this unique vantage point that I can appreciate Sunil's skill for preparing students to be productive members in the scientific community. He spent much time and effort training me in spectroscopy. He is a gifted teacher and has a true passion for teaching both in the classroom and in the lab. I am very appreciative for all his encouragement, patience, and advice.

I also thank Professors Michael Cascio, David Waldeck, and Stephen Weber for serving on my committee, and for providing advice and support throughout my graduate career. I am very appreciative to Professor Michael Trakselis for his assistance as the mentor of my Proposal. Neither of my projects would have been possible without the contributions from our collaborators, Professors Linda Jen-Jacobson and Michael Cascio and their groups. I thank Jacqueline Townsend, Dr. Paul Sapienza, and Lance Mabus from the Jen-Jacobson group for generating the mutants for the EcoRI project. I also thank Dr. Tommy Tillman, Emily Wickline, and Liz Brough from the Cascio group. Tommy was instrumental in training me in molecular biology techniques, and Emily and Liz worked tirelessly in the expression and purification of the glycine receptor.

I thank all past and present group members for their friendship and support. In particular, I am grateful to have had the opportunity to work with Drs. Marco Bonora and Soraya Pornsuwan. In addition to becoming amazing friends, Marco diligently trained me on the spectrometer, and Soraya was our programming guru. I will always fondly remember the wonderful times we shared as the “founding members.” I am also appreciative of Zhongyu Yang for his help in the glycine receptor project, both in experiments and modeling. Yang is an incredible theorist and an asset to the group. I thank Dr. Sharon Ruthstein for an immeasurable amount of help in troubleshooting experiments, training me on the use of the CW resonator, and most importantly for well-timed coffee breaks. Jennifer Grzybowski, Courteny Balliet, Joshua Elder, and Nicole Barkley were all very bright students who contributed to the glycine receptor project as undergraduate researchers. I am very grateful to Jim Becker and his family for hosting our group during the holidays. We spent many wonderful Thanksgiving and Easter dinners with them, and they became a Pittsburgh home for the Saxena group. I am most appreciative to have worked with Jessica Sarver. It was a pleasure working with her on both of my projects. She is a smart and determined experimentalist, and a very close friend. The last few years would not have been nearly as productive or enjoyable without her.

Finally I thank my family and friends for their love and encouragement. I would not have made it through the tough times without my parents, Kimberly and Peter Boehm, and Neil Donovan. They never questioned my ability to succeed, even in the times when I did, and I draw incredible strength from each of them. I also truly treasure my amazing group of friends from the Chemistry Department. Brianne, Aparna, Christina, Sruti, and Jessica have become friends for life.

## **1.0 INTRODUCTION**

### **1.1 ABSRACT**

Structural biologists and biophysicists are increasingly interested in correlating the conformational motions in proteins with their function. Proteins are responsible for carrying out cellular processes, and as such the determination of their structure and function leads to a deeper understanding of human pathology and more effective drug discovery. A variety of methods are well established for probing the atomic level structural details of proteins, including X-ray crystallography, nuclear magnetic resonance (NMR), Förster resonance energy transfer (FRET), and electron spin resonance (ESR). However, some classes of proteins elude traditional experimental methods. To date, less than 1% of the ~52,000 protein structures deposited in the Protein Data Bank are membrane proteins. The lack of experimental structural data on such a biologically important class of proteins suggests a need for alternative techniques for structure elucidation. ESR is well suited to provide both structural and dynamical data on systems that are historically difficult to characterize by other means.

## 1.2 SITE-DIRECTED SPIN LABELING FOR ESR

ESR requires the presence of an unpaired electron. For protein systems containing no paramagnetic species, which includes most proteins with the exception of metalloproteins, an unpaired electron must be introduced. In 1989, seminal work in the laboratory of Wayne Hubbell transformed Electron Spin Resonance spectroscopy into a powerful new tool for protein research. Hubbell introduced the implementation of site-directed mutagenesis for routine site-specific incorporation of ESR-active labels in proteins. This technique, called site-directed spin labeling (SDSL), is now an established method for structural and dynamical measurements of soluble proteins as well as many membrane proteins.<sup>[1,2]</sup>

The power of SDSL lies in the ability to attach a label to virtually any accessible residue on a protein. Using standard molecular biology methods, one can replace the amino acid residue of interest with a cysteine.<sup>[3-6]</sup> After the protein is expressed and purified, it is reacted with a thiol-specific stable organic radical. The most widely used label is (1-oxy-2,2,5,5-tetramethylpyrroline-3-methyl)methanethiosulfonate, or MTSSL, which contains a single unpaired electron in the nitroxide moiety. MTSSL is covalently attached to the cysteine residue via a disulfide linkage. Figure 1 shows the route by which the label attaches to the residue. ESR experiments on proteins spin labeled by SDSL permits experiments on proteins over a large range of temperatures in sample conditions that are more physiologically relevant than other methods.

One of the most important features of SDSL is that the incorporation of the MTSSL typically causes minimal perturbation to the native structure of a protein. The nitroxide was shown to have little to no effect on the structure of bacteriorhodopsin<sup>[7]</sup> and systematic spin labeling of domains of the T4 lysozyme had little effect on either the stability or structure.<sup>[8]</sup>

Finally, in many cases, ESR on spin labeled proteins provided experimental data consistent with a structure determined by X-ray crystallography.<sup>[9]</sup>

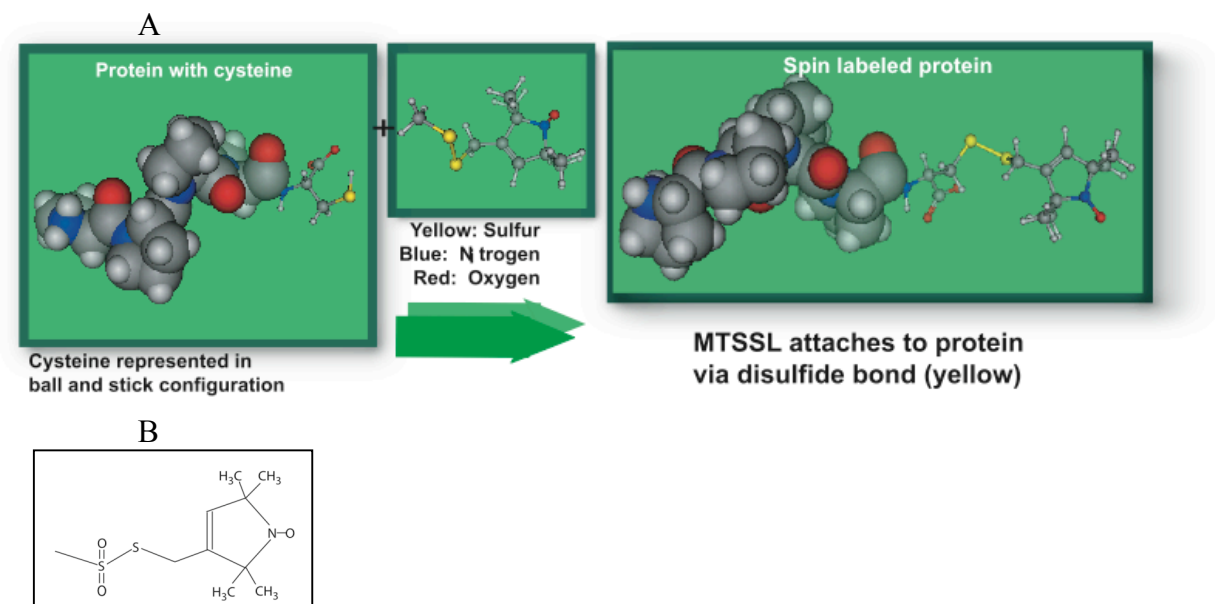


**Figure 1.1** Site-directed spin labeling of a protein. A. Methanethiosulfonate, MTSSL attaches to the free cysteine of the protein. A disulfide bond is formed. B. Structure of MTSSL.

### 1.3 DETERMINATION OF STRUCTURE AND DYNAMICS BY SDSL ESR

In general, ESR experiments on spin labeled proteins can be divided into those that provide either structural or dynamical data, summarized in Figure 2. The ESR spectrum is very sensitive to changes in the nitroxide environment, and thus it is an excellent method for probing the local environment of specific residues (Figure 2b). The ESR line shape can be used to probe conformational motions, backbone fluctuations, and the presence of transient structural conformations. Solvent accessibility experiments and line shape analysis can provide information about secondary structures and the relative orientation of domains in a membrane or at the surface of a membrane. Continuous Wave (CW) ESR experiments have been used to characterize the transmembrane segments and the protein-membrane interface of a potassium channel, the mechanisms of assembly of annexins, protein-protein interactions, the docking of proteins with a lipid membrane, secondary structures and conformational changes of bacteriorhodopsin, and the large amplitude domain motions of the T4 lysozyme, in addition to many other systems.<sup>[10-23]</sup> Membrane associated proteins, including ion channels, have also been investigated by ESR. Perozo and coworkers have spin labeled entire domains of a potassium channel, KcsA, and a mechanoselective ion channel, MscL. Differences in the line shape from each mutant were analyzed in order to determine secondary structures, tertiary interactions, depth of immersion, and distances between paramagnetic centers.<sup>[24-32]</sup> The MscL channel was probed in both the open and closed state by varying membrane composition.<sup>[28, 31]</sup> In all these cases, the line shapes of CW ESR spectra reported on the local dynamics of the proteins at the position of the spin label.

Although information about the *local* environment of the spin label can provide tremendous information about structure and dynamics of a protein, oftentimes proteins undergo

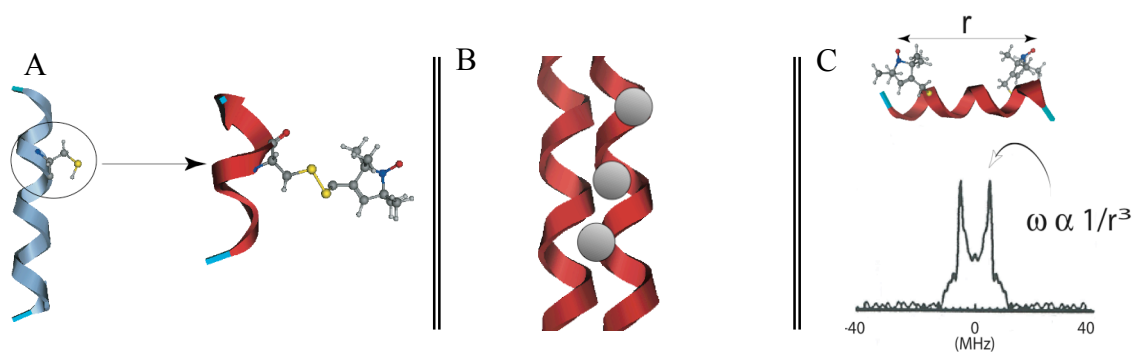


**Figure 1.2** (A) Site-directed mutagenesis in tandem with site-directed spin labeling allows for the selective attachment of an ESR active label to virtually any position in the protein sequence. (B) The CW lineshape is sensitive to the local environment of the spin label, and can be used to assess the extent of tertiary interaction, as well as other structural and dynamical information. (C) The distance between two spin labels, up to  $\sim 70$  Å, can be measured using pulsed ESR distance methods.

conformational changes as a result of large domain motions. The amplitude of protein domain motions can be directly quantified by measuring the changes in distances between two spin labels on a protein (Figure 2c). Although ESR distance measurements do not provide high-resolution three-dimensional structures of proteins, the technique has some notable advantages over other methods. While X-ray crystallography is undoubtedly a powerful tool in structural biology (it accounts for 90% of the determined protein structures in the Protein Data Bank), the structures do not necessarily reflect the native protein conformation in solution. Membrane proteins pose a challenge for crystallographers, since it is difficult to form crystals of proteins in detergent. NMR is often used to solve high resolution structures of proteins that are not crystallizable, but this technique is limited to proteins <60 kDa and requires very high protein concentrations (~0.5-1.0 mM). Many proteins are excluded for NMR analysis by these sample requirements. FRET experiments can be used to measure long-range distance constraints and requires very low sample concentrations. However, FRET requires knowledge of the orientations of the fluorophores, which can make data analysis difficult. Also, the fluorophore labels are generally much larger than nitroxide labels. Larger labels suffer from poorer accessibility to the residue of interest and higher perturbation to the system. Fluorescence distance measurements require a donor and an acceptor label, further complicating sample preparation.

ESR distance methods, such as Double Electron-Electron Resonance (DEER) and Double Quantum Coherence (DQC) ESR are capable of detecting the weak electron-electron dipolar interactions between two spin labels<sup>[33-43]</sup> in order to determine the inter-spin distances in the ~20-70 Å range. Access to this range of distances is crucial for elucidating structural and

conformational changes in proteins, and in particular, membrane proteins. The DEER experiment has been shown to be an effective experiment for measuring inter-spin distances in a variety of biological systems including membrane proteins,<sup>[12, 13]</sup> soluble proteins,<sup>[14, 15]</sup> peptides,<sup>[16]</sup> oligonucleotides,<sup>[17, 18]</sup> synthetic oligomers,<sup>[19-21]</sup> and protein-DNA complexes. The focus of this thesis is on the measurement of distances in proteins by DEER-ESR. The following sections provide details about extracting distances, distance distributions, and the average number of coupled spins from the DEER data.

## 1.4 DEER-ESR

In order to understand the ESR spectrum, it is necessary to consider the spin Hamiltonian. The equation for the spin Hamiltonian gives details of the interactions of electron and nuclear spins with the magnetic field and with each other. When the nitroxide undergoes fast motion ( $10^8$  to  $10^{10}$  s<sup>-1</sup>) the  $g$  and hyperfine tensors are averaged out and the Hamiltonian is

$$\hat{H} = g\beta_e B_z \hat{S}_z + a \hat{I}_z \hat{S}_z \quad [1]$$

where  $g$  is the electron  $g$  factor,  $\beta_e$  is the Bohr magneton for an electron,  $a$  is the hyperfine splitting constant, and  $S_z$  and  $I_z$  are the electron and nuclear spin operators, respectively. The first term of Eq. 1 is the Zeeman interaction of the electron spins, which is responsible for breaking the degeneracy of the electron spin energy levels in the presence of a magnetic field, as shown in red in Figure 3. The second term in Eq. 1 is the hyperfine interaction between the electron and nuclear spins on a nitroxide. The hyperfine interaction further splits the energy levels for a total of six states for a nitroxide, as shown in blue in Figure 3. The Zeeman and

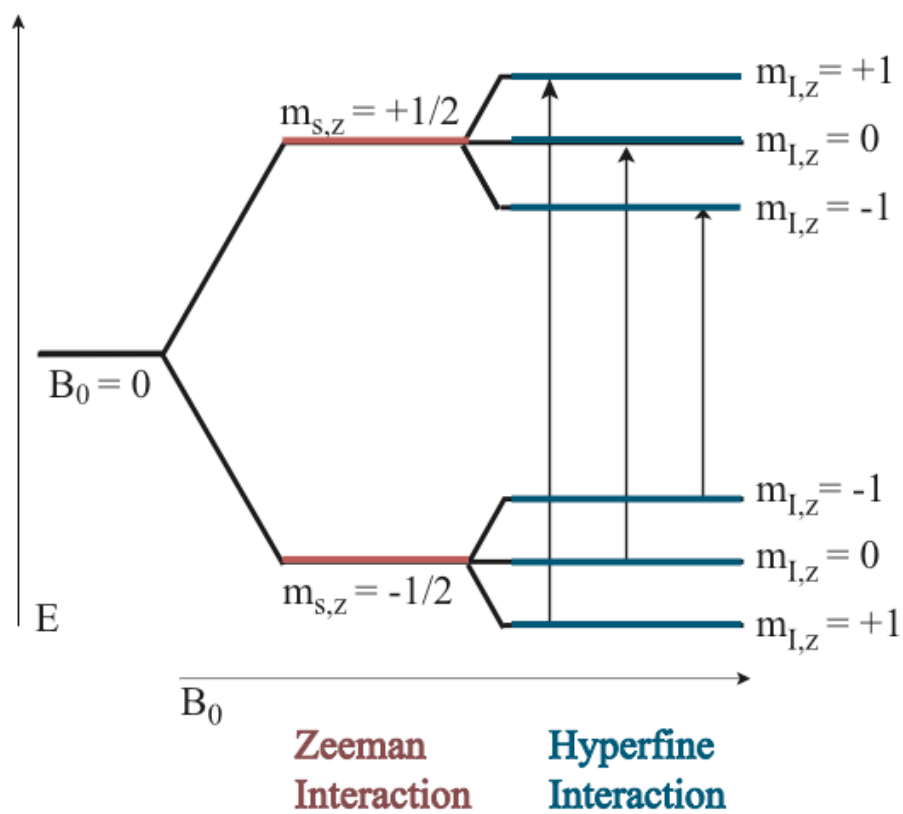


**Figure 1.3** Energy level diagram for nitroxides. In the presence of the external magnetic field, the degeneracy of the energy levels for the spins is broken. These states are further split by the nuclear spin as  $2I + 1$ .

hyperfine interactions produce the typical three line nitroxide spectrum. Figure 3 shows the energy level diagram for nitroxides, with an electron spin  $S$ , of  $1/2$  and a nuclear spin  $I$  of  $1$ . Since there are  $2S+1$  orientations, two linearly independent wavefunctions result,  $|\alpha\rangle$  and  $|\beta\rangle$ . The wavefunctions  $|\alpha\rangle$  and  $|\beta\rangle$  are quantized by the azimuthal quantum number,  $m_{s,z}$ . In the absence of the magnetic field, these states are degenerate. The Zeeman interaction lifts the degeneracy, and now  $|\alpha\rangle$  is higher in energy than  $|\beta\rangle$ . The hyperfine interaction further splits each state by  $2I+1$  giving six total states,  $m_{I,z}$ . The selection rules,  $\Delta M_{z,S} = \pm 1$  and  $\Delta M_{z,I} = 0$  dictate that only three transitions may occur, which are represented as arrows in Figure 3.

If a molecule is doubly labeled with two nitroxides, a dipole-dipole interaction between the two unpaired electrons must be added to the Hamiltonian. The new term,  $H_{DD}$ , is

$$H_{DD} = D/2(3 \cos^2\theta - 1)(S_z^2 - S^2/3), \quad [2]$$

and

$$D = \frac{g_1 g_2 \beta^2 \mu_0}{4 \pi \hbar r_{12}^3}, \quad [3]$$

where  $r$  is the distance between the two unpaired electrons, and  $\theta$  is the angle between the external magnetic field and the inter-spin vector as shown in Figure 4a.

The DEER experiment is a two-frequency pulsed ESR experiment used to isolate the distance dependent dipole-dipole coupling. The weak dipole-dipole coupling is much smaller than the unresolved hyperfine coupling for inter-spin distance greater than  $20 \text{ \AA}$ . The pulse sequence for the 4-pulse DEER experiment is shown in Figure 5a. A  $\pi/2$  pulse is applied in the  $\nu_a$  frequency and excites 'A' spins as shown in the excitation profile of the observer pulse in Figure 5b.

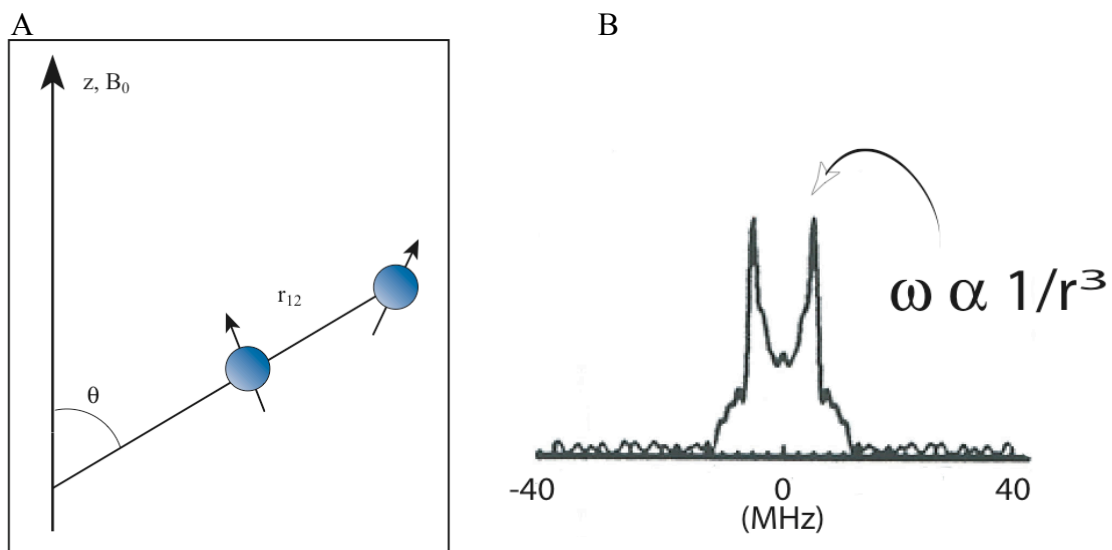


**Figure 1.4.** The dipolar interaction. (A) Two nitroxides in a magnetic field. Electron spins from two nitroxides are labeled 1 and 2. (B) Pake pattern showing the frequency of the dipolar interaction.

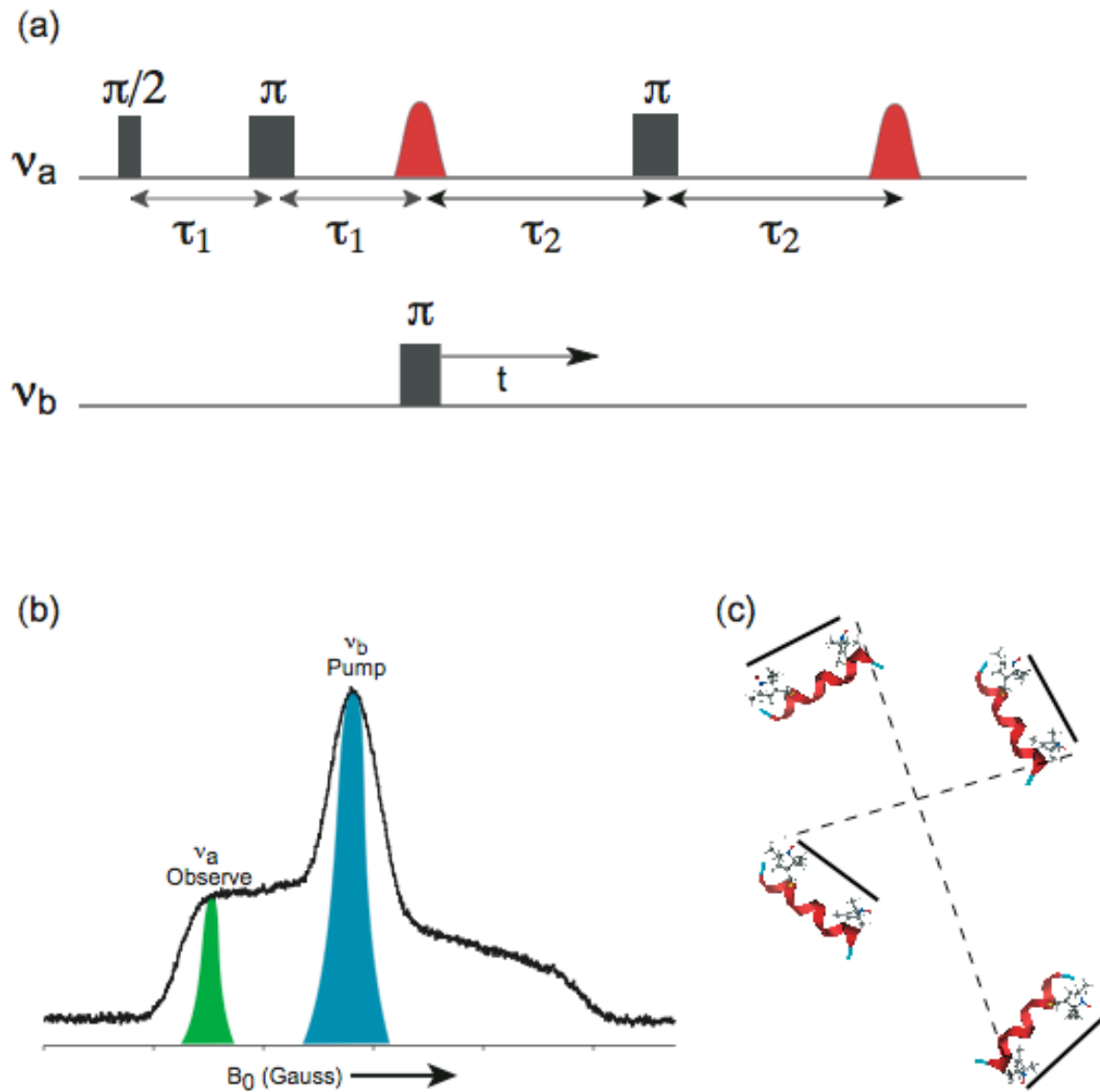


**Figure 1.5** (A) Pulse sequence for the 4-pulse DEER experiment. (B) Excitation profile of the pump and observe pulses. (C) Examples of intramolecular (solid lines) and intermolecular (dotted line) interactions in a sample of doubly labeled peptides.

The first  $\pi/2$  pulse rotates the magnetization of the A spins into the xy plane. Next, a  $\pi$  pulse is applied at a time  $\tau_1$ , which refocuses the spins, and a Hahn echo forms at  $2\tau_1$ . The third pulse is a  $\pi$  pulse at a second microwave frequency,  $\nu_b$ , with an excitation profile corresponding to the pump pulse in Figure 5b. This pulse, which occurs at a variable time,  $t$  during the refocusing of spins A, inverts the magnetization of the B spins. The inversion of the B spins causes a change in the local magnetic field experienced by the A spins. A final  $\pi$  pulse at  $\nu_a$  refocuses the spin magnetization of the A spins. The integrated intensity of the stimulated echo modulates at a frequency of the dipolar interaction as a result of the flipping of B spins at a variable time.

In a multi-spin system, the resulting signal can be written as the product of two contributions:

$$V(t) = V_{\text{int } ra} * V_{\text{int } er}. \quad [4]$$

The  $V_{\text{intra}}$  term describes the intramolecular signal due to the interaction of spins in a single system, and the  $V_{\text{inter}}$  term describes the signal due to the homogeneous distribution of spins in the sample. Figure 5c illustrates the origins of the intramolecular and intermolecular interactions in a doubly spin labeled sample. The  $V_{\text{intra}}$  signal is given by<sup>[44]</sup>

$$V_{\text{int } ra} = \frac{1}{n} \left\langle \sum_{A=1}^n \prod_{\substack{B=1 \\ B \neq A}}^n (1 - p_b(\cos(\omega_{AB}t))) \right\rangle, \quad [5]$$

where  $n$  is the number of spins per system,  $p_b$  is the fraction of B spins excited by the pump pulse, and  $t$  is the time delay of the pump pulse. The dipolar splitting,  $\omega_{AB}$  is defined as

$$\omega_{AB} = \frac{\beta_e^2 g_A g_B}{\hbar} \frac{(3\cos^2 \theta_{AB} - 1)}{r_{AB}^3}, \quad [6]$$

where  $g_A$  and  $g_B$  are the g factors for the A and B spins,  $r_{AB}$  is the distance between the A and B spins, and  $\theta_{AB}$  is the angle formed by the interspin vector and the external magnetic field. Hence, the signal arising from the intramolecular interaction is due to the modulation of the distance dependent dipolar interaction. Figure 4b shows the relationship between the frequency of the dipolar interaction and the distance between the two spins. In a powder sample, all orientations of  $\theta$  are spanned and one obtains a very characteristic pattern, called the Pake pattern.<sup>[45]</sup> Due to the use of finite lengths of pulses in the experiment and the presence of a distribution in distances, the peaks due to  $\theta=90^\circ$  are typically emphasized. The experiment then provides a direct measurement of inter-spin distances.

Since the  $V_{inter}$  signal is due to the homogeneous, random distribution of spins in the sample, the distance dependent modulation is averaged out. The  $V_{inter}$  signal can be written as

$$V_{inter} = \exp(-kCp_b t), \quad [7]$$

where C is the concentration of A spins participating in the intermolecular interaction and k is

$$k = \frac{8\pi^2 \beta_e^2 g_A g_B}{9\sqrt{3}\hbar}. \quad [8]$$

Extraction of the distances from the DEER signal requires separation of the  $V_{intra}$  signal from the  $V_{inter}$  signal in order to eliminate contributions from spins on neighboring molecules. This can be achieved by dividing the total signal,  $V(t)$  by a background correction factor. The most accurate background correction is an experimentally determined background function from a singly labeled sample. Oftentimes, as is the case with oligomeric proteins, it is not possible to obtain the intermolecular decay from a singly labeled sample experimentally. In these situations, the intermolecular background signal must be fit to an appropriate exponential function. For distances shorter than 40 Å, separation is not typically problematic. Background correction for

systems containing distances longer than 40 Å are more difficult because the dipolar modulation decays more slowly. A sufficiently long dipolar evolution time must be collected ( $\tau_2$  in Figure 5a) so that the intermolecular component to the signal can be distinguished from the intramolecular signal.

For a sample of spin labeled molecules homogeneously distributed, the intermolecular component of the signal may be fit to the background function

$$B(t) = \exp(-kt^{d/3}), \quad [9]$$

where  $k$  describes the density of the spins, and  $d$  represents the dimensionality of the distribution. For most samples, molecules are distributed homogeneously in three dimensions, and  $d=3$ . In some cases, membrane proteins are restricted to two dimensions, and  $d=2$ .

After background correction, the signal may be simulated to extract distances and distance distributions. The generation of a distance distribution function from the DEER signal,  $V(t)$  is considered an ill-posed problem because many different distance distribution functions can correspond to simulated  $V(t)$  signals that are in reasonable agreement with the experimental  $V(t)$  signal. Recently, the Tikhonov regularization has been used to invert the experimental time domain signal in order to obtain a distance distribution function. The Tikhonov regularization optimizes the resolution of the distance distribution function while minimizing artifacts due to noise in the time domain signal using a regularization parameter,  $\alpha$ . The L-curve criterion is used to mathematically determine the most appropriate value of  $\alpha$ . The L-curve criterion utilizes an L-shaped plot that optimizes both the mean square deviation and the smoothness of the distance distribution function. If the  $\alpha$  value is too small, the distance distribution is under smoothed, and artificial peaks are produced. Conversely, inappropriately large  $\alpha$  values lead to over smoothing and over broadened peaks. Selecting the  $\alpha$  value in the “corner” of the L-curve

strikes the best compromise between artifact suppression and resolution of the peaks in the distribution function. In chapters 2 and 3 of this thesis, all DEER time domain data were inverted to obtain distance distribution functions using the Tikhonov regularization in the DeerAnalysis2006 program.<sup>[46]</sup> Further, details of the Tikhonov regularization are available in the literature.<sup>[47, 48]</sup>

## 1.5 SPIN COUNTING BY DEER-ESR

In addition to measuring inter-spin distances, the DEER signal can also be used to determine the number of unpaired electrons in a molecule. In a series of papers, Tsvetkov and coworkers showed that the modulation depth of the DEER signal is directly related to the number of coupled spins.<sup>[49-51]</sup> This is particularly useful for determining the aggregation states of some peptides or the degree of oligomerization in a protein complex. The limiting value of the background corrected DEER signal corresponding to

$$V_p = V_{\text{int ra}} (T \rightarrow \infty) \quad [10]$$

is related to the number spins by the equation

$$V_p = (1 - p_b)^{n-1}, \quad [11]$$

where  $n$  is the number of spins in the molecule, and the fraction of B spins excited by the pump pulse,  $p_b$ , can be determined experimentally using a standard biradical. Figure 6 shows the  $V_{\text{intra}}$  signal by Tsvetkov and coworkers for several peptide samples with different mean number of spins per aggregate.<sup>[49]</sup> As the doubly labeled peptide aggregates are diluted with unlabeled peptides, the mean number of spins per aggregate decreases, and hence  $V_p$  increases.

In 2007, Schiemann and coworkers experimentally verified the spin counting technique using well-characterized synthesized polynitroxide radicals.<sup>[44]</sup> They prepared several model radicals designed to represent a variety of aggregation states and geometric arrangements of nitroxides. Since biological systems may consist of a mixture of oligomeric states in equilibrium, it is worthwhile to consider the accuracy with which the mean number of oligomers can be determined. The authors found that Eq. 11 is only valid when the number of spins is equal in each molecule of the sample, and that the accuracy of  $n$  depends on the error of  $V_p$ . For a sample containing a mixture of spin labeled species, contributions to  $V_p$  from each spin labeled species should be taken into account.  $V_p$  can be expressed as the weighted sum

$$V_p = \sum_i \chi_i V_{pi} , \quad [12]$$

where  $\chi_i$  is the fraction of spins in the respective spin labeled species giving the signal  $V_{pi}$ . In samples where there is a large difference in the number of couple spins per molecule, an additional relaxation scaling factor is needed to take into account the difference in the transverse relaxation time,  $T_2$  for each species. Equation 12 can be modified to include this scaling factor such that  $V_p$  now becomes

$$V_p = \frac{\sum_i s_i \chi_i V_{pi}}{\sum_i s_i \chi_i} , \quad [13]$$

and  $s_i$  is defined as

$$s_i = \frac{A_{REi} / A_{HEi}}{A_{RE_{mono}} / A_{HE_{mono}}} . \quad [14]$$

In Eq. 14, the relaxation scaling factor is estimated by dividing the ratio of the refocused echo amplitude,  $A_{REi}$  and the Hahn echo amplitude,  $A_{HEi}$  for each pure spin labeled species in the mixture by the ratio of the refocused echo amplitude and the Hahn echo amplitude for a monolabeled species.

In practice, it is not always possible to know the composition of the sample. Additionally, for the case of oligomeric proteins, it may be difficult to obtain a monolabeled sample or separate the different spin labeled species in order to measure the echo amplitudes of each pure species. For mixtures of unknown composition, in theory it is possible to measure  $V_p$  at several values of  $p_b$ . If  $p_b$  is known and  $V_{pi}$  is experimentally determined, the number of spins in each oligomer can be determined by solving simultaneous equations.

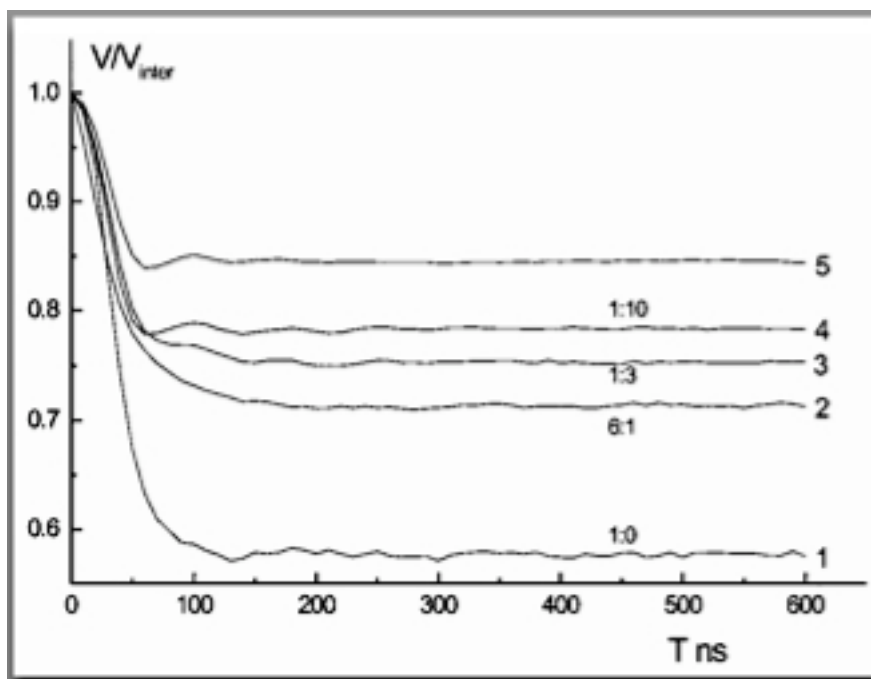


**Figure 1.6.** Dependence of  $V_{\text{intra}}$  on the number of coupled spins. As doubly labeled peptide aggregates are diluted with unlabeled peptides, the modulation depth decreases and  $V_p$  increases. Figure taken from reference 49.

## **2.0 ELECTRON SPIN RESONANCE SHOWS COMMON STRUCTURAL FEATURES FOR DIFFERENT CLASSES OF ECO-RI-DNA COMPLEXES**

*Part of this chapter, written in collaboration with Jacqueline Townsend, Jessica Sarver, Paul Sapienza, Linda Jen-Jacobson, and Sunil Saxena, has been published in Angewandte Chemie International Edition, 2008, V. 47 pages 10192-10194.*

### **2.1 ABSTRACT**

In this chapter, we describe how site-directed spin labeling and double electron-electron resonance (DEER) ESR can be used to probe the disorder-to-order transition in a restriction endonuclease, EcoRI as it binds to different sequences of double stranded DNA. Three mutants of EcoRI were constructed (R131C, S180C, and K249C-S180C) in order to investigate structural changes in the arm region, which is known to be critically involved in DNA recognition. Distance constraints were measured, and the average distance remained the same for each mutant bound to different complexes. These data suggest that the average structure of the arm region is preserved for different DNA complexes with EcoRI.

## 2.2 INTRODUCTION

We show that the EcoRI restriction endonuclease binds different classes of DNA sites in the same binding cleft. EcoRI generates widespread interest because it exhibits an extraordinary sequence selectivity to carry out its function of cleaving incoming foreign DNA without causing potentially lethal cleavage of cellular DNA. For example, EcoRI binds to its correct recognition site GAATTC up to 90,000-fold better than to miscognate sites that have one incorrect base pair.<sup>[52, 53]</sup> The ~650 specific sites in the *E. coli* genome are protected from cleavage by double-strand methylation. The ~21,000 miscognate sites are not methylated, but are still cleaved by EcoRI with a second-order rate constant that is  $\sim 10^9$ -fold lower.<sup>[52, 53]</sup> EcoRI forms only non-specific complexes with no cleavage at sites that differ from GAATTC by two or more base pairs.<sup>[1,2]</sup>

In order to understand the source of such high specificity, it is necessary to determine how the structures of EcoRI complexes differ at specific, miscognate (5/6 bp match), and non-specific ( $\leq 4/6$  bp match) DNA sites. This effort is timely given the extensive genetic, biochemical and biophysical data on EcoRI.<sup>[52-60]</sup> Footprinting results<sup>[52]</sup> suggest that the three classes of complexes are “structurally” distinct, and thermodynamic profiles ( $\Delta G^\circ$ ,  $\Delta H^\circ$ ,  $\Delta S^\circ$ ,  $\Delta C_p^\circ$ )<sup>[54, 55]</sup> suggest that the specific complex has more restricted conformational-vibrational mobility of the protein and DNA. There are crystal structures of the free protein,<sup>[57]</sup> and the metal-free specific protein-DNA complex.<sup>[57, 58]</sup> Miscognate and non-specific complexes however, have not been readily accessible to crystallographic analysis. Indeed, for the ~3600 known restriction endonucleases, there are currently 73 crystal structures of 38 distinct enzymes in complex with specific DNA. However, there are only 4 structures of miscognate or non-specific complexes in the protein data bank.<sup>[61]</sup> NMR experiments are also not possible for the

complexes for several reasons. At 62 kDa, excluding DNA, EcoRI is at the size limit for resolution by NMR. Also, NMR requires protein concentrations of  $\sim 1.0$  mM, and EcoRI precipitates at such high concentrations. In this chapter, the utility of pulsed ESR distance measurements to shed light on miscognate and non-specific complexes is demonstrated.

## 2.3 METHODS

- **ESR Experimental Details**

All ESR experiments were performed on a Bruker EleXsys E580 CW/FT X-Band ESR spectrometer using the Bruker X-Band ER 4118X-MS2, MS3, and MD5 split ring resonators. For the R131C and the K249-S180C samples, between 10 and 25  $\mu\text{L}$  were used. The protein concentrations ranged from 75 to 80  $\mu\text{M}$ , and the samples were prepared in a buffer containing 30 % glycerol as a cryoprotectant. With these concentrations and volumes, a dipolar evolution time of  $\sim 1.5$ - 2.5  $\mu\text{s}$  could be collected in the DEER experiment so that distances less than 40  $\text{\AA}$  could be easily accessed. For the S180C mutants, a distance in the range of 60-70  $\text{\AA}$  was anticipated from the crystal structure. Therefore, higher concentrations, volumes, and phase memory times were required. For the S180C, mutant  $\sim 90$   $\mu\text{L}$  of sample in 30% deuterated glycerol, 65% deuterated water, and 5% protonated water was used. The protein concentrations for the S180C samples were 180  $\mu\text{M}$  (specific) and 120  $\mu\text{M}$  (nonspecific). Given the need for such exhaustive protein concentrations and volumes, only the specific and the non-specific complexes of S180C were studied so that comparisons between the most disparate complexes can be made.

In all cases, excess DNA, appropriate salt concentrations (0.22 M), and pH were used to ensure that virtually all of the protein was bound to DNA.<sup>[62]</sup> For example, for the wild-type EcoRI, DNA:protein ratios of 4:1, 12:1, and 17:1 for the specific, miscognate, and nonspecific complexes, respectively, ensure that at least 99% of the sample exists as the protein-DNA complex. We assayed the protein-DNA complex after the ESR experiment via molecular sieve (gel filtration) chromatography, and all the protein migrated in the position of a dimer-DNA complex. Experiments on free protein were not carried out because we were primarily interested in comparing distinct protein-DNA complexes and not in mapping out changes between free protein and DNA-bound protein. The latter question is technically inaccessible by ESR, because at the concentrations required for spectroscopy the free protein forms only tetramers, whereas in the protein-DNA complexes there are only protein dimers. Binding assays and ESR experiments were carried out in the absence of catalytic cofactor ( $Mg^{2+}$ ); highly specific binding occurs even under such conditions.<sup>[56]</sup>

The R131C samples were flash frozen by plunging the capillaries into liquid nitrogen, and the S180C and K249C-S180C samples were flash frozen by plunging the capillaries into liquid nitrogen cooled propane. The R131C and K249C-S180C experiments were performed at 80 K, whereas the S180C experiments were performed at 40 K. The temperature was stabilized using an Oxford IT C605 temperature controller and ER 4118 CF gas flow cryostat. An ASE TWTA provided an output power of 1 kW.

The 4-pulse DEER sequence<sup>[38]</sup>  $(\pi/2)v_a-\tau_1-(\pi)v_a-t'-(\pi)v_b-\tau_1+\tau_2-t'-(\pi)v_a-\tau_2$ -echo was used with a two-step phase cycle for baseline correction. For the R131C specific, miscognate, and non-specific samples,  $\pi/2$  and  $\pi$  pulses were 24 and 48 ns respectively,  $\tau_1$  was 200 ns, and  $\tau_2$  was chosen to be 2.6  $\mu$ s based on the phase memory time ( $T_m$ ). The observer frequency was placed

at the maximum of the nitroxide spectrum and the pump frequency was  $\sim 70$  MHz away at the maximum of the low field component, as shown in Figure 1. The inter-pulse delay,  $t'$ , was incremented 10 ns, and the integrated echo intensity was collected for 256 points. Total data acquisition times were 24-36 hours.

The  $\pi/2$  and  $\pi$  pulses for the K249C-S180C specific and miscognate complexes were 16 and 32 ns, respectively. We used 24 and 48 ns pulse lengths for the non-specific complex to eliminate the proton ESEEM modulation. As before, the  $\tau_1$  pulse delay was 200 ns, but  $\tau_2$  was shortened to 1.6  $\mu$ s because the K249-S180C complexes exhibited a shorter  $T_m$ . The pump frequency for these samples was placed at the maximum of the nitroxide spectrum, and the observer frequency was  $\sim 65$  MHz away at the low field component. The inter-pulse delay,  $t'$ , was incremented 12 ns and the integrated echo intensity was collected for 128 points. Total data acquisition times were 28-72 hours.

For the S180C specific and non-specific samples,  $\pi/2$  and  $\pi$  pulses were 16 and 32 ns in length respectively. In order to accurately assess the zero time, the  $\tau_1$  pulse delay was increased to 400 ns, and the pump pulse began 300 ns before the maximum of the echo. The pump frequency was placed at the maximum of the nitroxide spectrum, and the observer frequency was  $\sim 70-75$  MHz away centered at the low field component. The inter-pulse delay,  $t'$ , was incremented 10 ns and the integrated echo intensity was collected for 512 points. The total data acquisition time for the S180C samples was 20-30 hours.

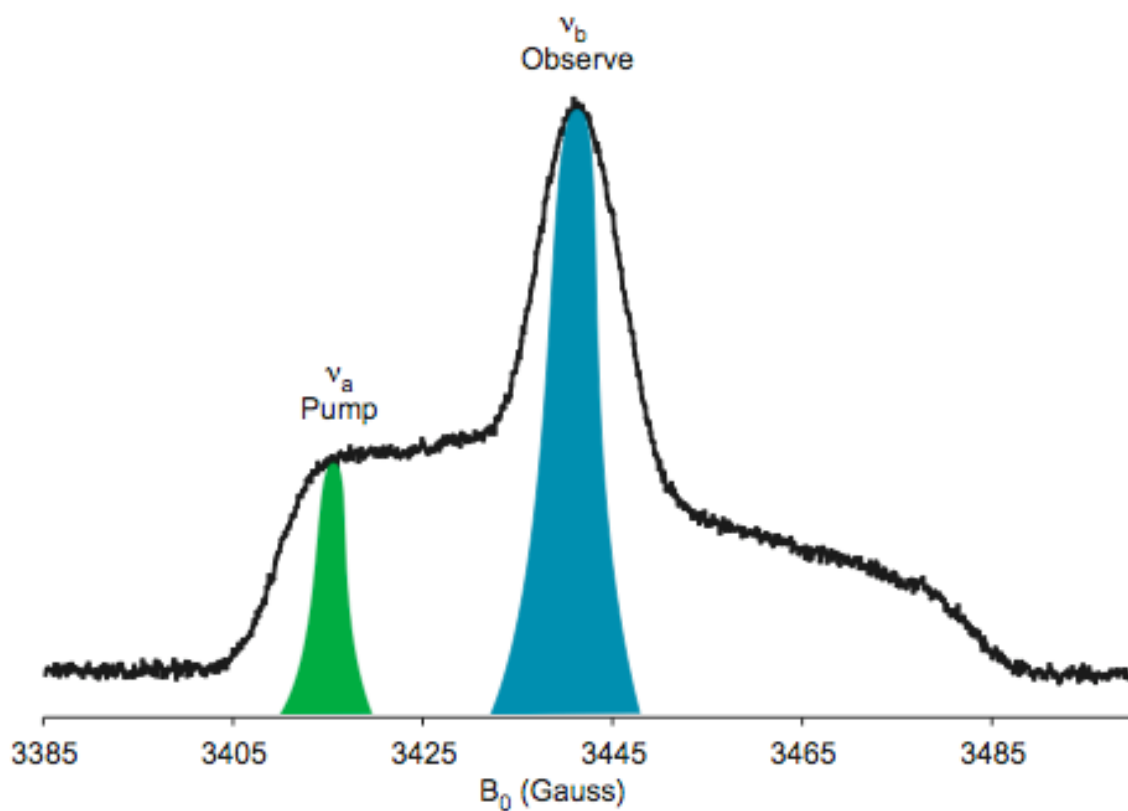


**Figure 2.1** Excitation profile of the pump and observe frequencies shown for the R131C complexes. All DEER-ESR experiments for the R131C DNA complexes were performed with the observer frequency placed at the maximum of the nitroxide spectrum, as shown here. For the S180C and K249C-S180C complexes, the pump frequency was placed at the maximum of the nitroxide spectrum, and the observer frequency was placed at the center of the low-field component.

- **Data Analysis**

Processing and distance distribution analysis of all time domain DEER data were performed using the DeerAnalysis2006 program.<sup>[46]</sup> Contributions to the signal due to intermolecular interactions were subtracted out by fitting approximately the last 65-75% of points to an exponential function assuming a homogeneous three-dimensional distribution. The Tikhonov regularization method was used to obtain the distance distribution functions, and the L-curve criterion was used to find the best regularization parameter,  $\alpha$ . A value of  $\alpha=100$  was appropriate for all samples except the R131C NS, for which 1000 was used. Based on the resolution, the error in the distances is estimated to be <10 % for each measurement.

- **DNA Binding by Mutant Proteins**

In order to confirm that the mutant proteins and their spin-labeled derivatives exhibit binding affinities similar to that of the wild-type protein, equilibrium association constants ( $K_A$ ) were determined using a standard filter binding assay.<sup>[62]</sup> We used a 22 base-pair <sup>32</sup>P end-labeled DNA substrate containing the cognate (i.e. specific) site GAATTC, with the sequence, GGGCGGGCGAATTCGCGGGCGC.

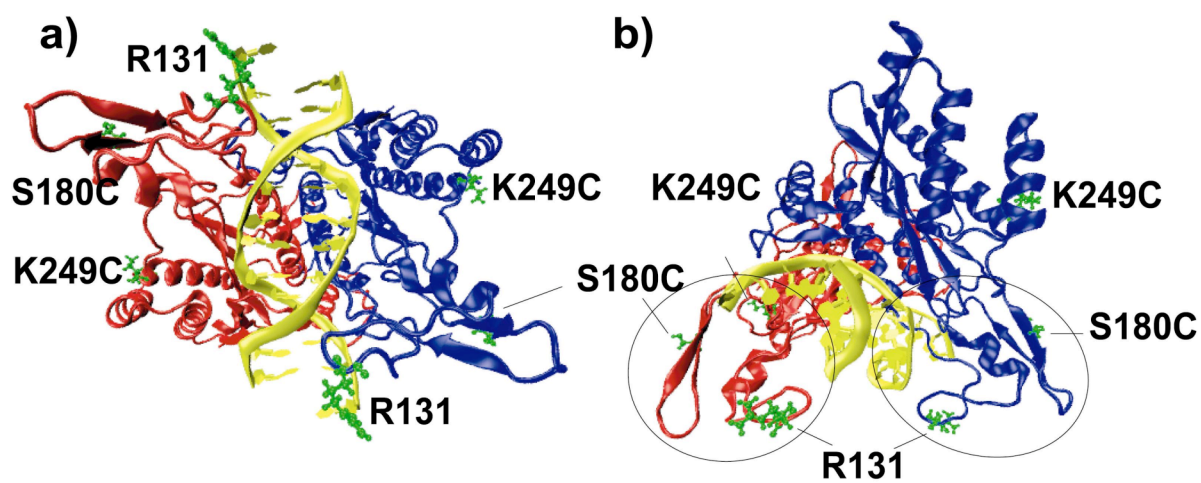
## 2.4 RESULTS AND DISCUSSION

Figure 2 shows the structure of the EcoRI specific complex.<sup>[57, 58]</sup> The protein contains a large, relatively rigid and structured globular “main” domain and a smaller "arm" region. The protein arms are invisible in the free protein<sup>[57]</sup> but become ordered and enfold the DNA in the specific complex.<sup>[53, 55]</sup> Ethylation interference footprinting experiments have been used to identify phosphate groups necessary for DNA to bind to EcoRI. Ethylation interference footprinting indicates that the protein-phosphate contacts are different for the specific and miscognate complexes of EcoRI.<sup>[63]</sup> Interestingly, residues in the arm region form new DNA contacts in the miscognate complex. No footprinting occurs for the non-specific complex. A change in the contacts suggests that the arms bind the DNA in different conformations.<sup>[52]</sup> Given that the arms are disordered and unresolved by X-ray for the free protein, and residues in the arm region of the miscognate complex are implicated in the footprinting experiment, it is clear that the arm region of EcoRI is critical for modulating specificity. We chose mutations that would probe the conformations of the inner and outer arms. Mutations R131C, S180C, and K249C-S180C were chosen based on the crystal structure.<sup>[57, 58]</sup> These sites are solvent accessible and therefore likely to spin label with minimal perturbation to protein structure. Residues R131 and S180 lie in the inner and outer arms, respectively. Residue K249 is in the main domain, which has very restricted movement<sup>[57]</sup> and acts as a reference point. Since EcoRI is a 62 kDa homodimer, single cysteine mutations provide two sites for spin labeling, and double mutations provide four sites.

The mutant proteins were spin labeled at the cysteines with the methanethiosulfonate spin label (MTSSL). There is an intrinsic cysteine at position 218, but it is buried. Figure 3 shows the field swept echo detected experiment for the spin labeled R131C non-specific complex and WT EcoRI. The normalized intensity of the WT signal may be compared to the signal from R131C to estimate the extent of labeling. Since the R131C non-specific complex is known to have ~100% labeling efficiency, we estimate that less than 10% of the cysteines in the WT EcoRI were labeled by the nitroxide even with a 100-fold molar excess of the spin label.

The mutant proteins and their spin labeled derivatives catalyze DNA cleavage and have DNA binding affinities similar to that of wild type EcoRI, indicating that they are functionally active. As seen in Table 1, mutant proteins (not spin labeled) S180C, R131C and K249C-S180C show very high binding affinities for the specific site. The decrease in binding upon mutation is very small when compared to the 51,000 and 96,000 fold decrease in binding of the wild type EcoRI to miscognate and non-specific DNA sites, respectively. The spin-labeled derivatives (e.g. S180Cspin ) were recovered from the sample cell after taking ESR spectra. Because these samples contained a large molar excess of 13-bp DNA, we cleaved the DNA by addition of  $Mg^{2+}$  then chelated the  $Mg^{2+}$  with EDTA. The binding assay was then carried out with  $^{32}P$ -labeled DNA. The unlabeled cleavage products are too short to interfere with the binding assay. Thus, spin-labeling and extensive handling have a combined effect on binding activity that is still modest.

DEER experiments<sup>[64]</sup> were performed on spin labeled S180C specific and non-specific complexes, and on R131C and K249C-S180C specific, miscognate, and non-specific complexes. The DEER experiment is now well established for measuring distance constraints in membrane proteins,<sup>[65, 66]</sup> soluble proteins,<sup>[67, 68]</sup> peptides,<sup>[69]</sup> oligonucleotides,<sup>[40, 70]</sup> and



**Figure 2.2** X-ray structure of the EcoRI specific complex. A) The bottom view shows monomers in red and blue. B) The side view illustrates the arm domain by circles. The DNA sequence is shown in yellow, and the residues mutated to cysteine are highlighted in green. Coordinates are from a highly refined version <sup>[6,7]</sup> of PDB entry 1CKQ.

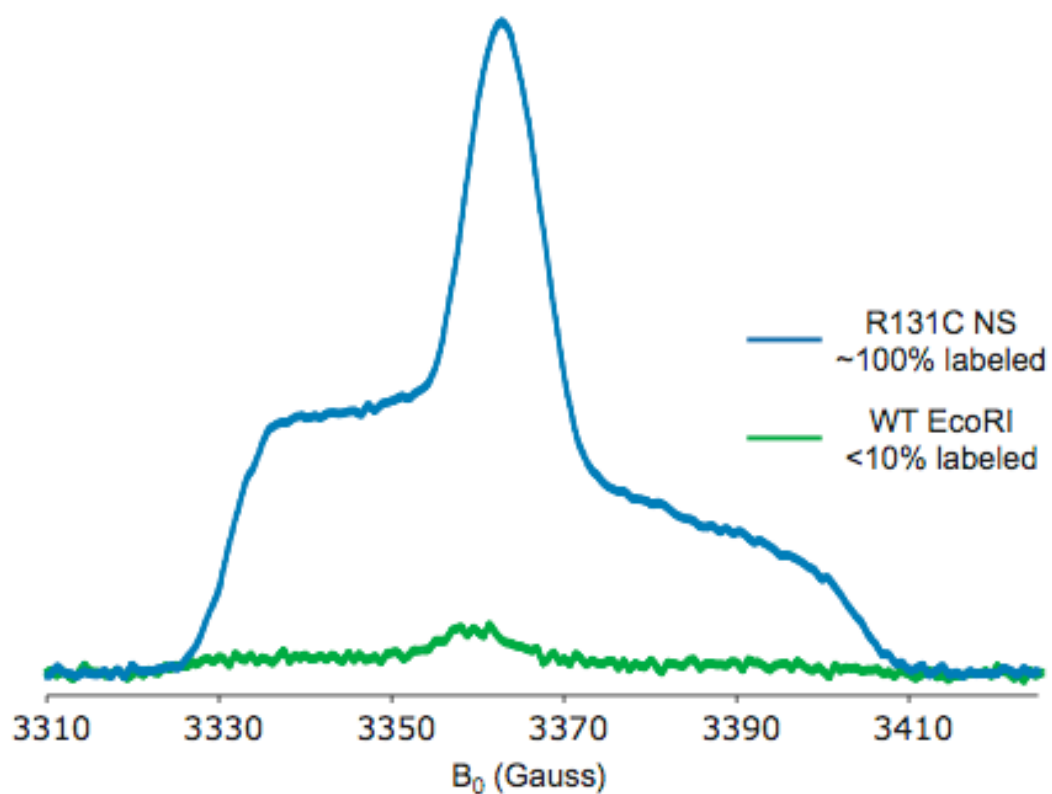


**Figure 2.3** A field swept echo detected experiment was used to estimate the labeling efficiency of the WT EcoRI specific complex (green). Compared to the signal for the R131C NS complex (blue), which had ~100% labeling efficiency, we estimate <10% of the cysteines at position 218 were modified with MTSSL.

**Table 2.1.** EcoRI equilibrium binding data to the specific site in 0.22M KCl, 20 mM Cacodylate, pH 7.3, at 21°C.

$\Delta\Delta G_{\text{bind}} = -RT \ln(K_{A,\text{mut}}/K_{A,\text{wt}})$ . The second wild-type sample was subjected to a mock spin-labeling reaction lacking the spin label reagent.

	$K_A(\text{M}^{-1})$	$\Delta\Delta G_{\text{bind}}^{\circ}$ (kcal/mol)	Relative binding ( $K_A \text{ WT}/K_A \text{ mutant}$ )
Wild type	$4.5 (+/- 1.4) \times 10^{10}$	0	1
Wild type mock spin-label	$3.0 \times 10^{10}$	0.2	1.5
S180C	$2.3 (+/-0.7) \times 10^{10}$	0.4	2
S180C <sup>spin</sup>	$1.8 (+/-0.4) \times 10^9$	1.9	25
K249C-S180C	$2.3 (+/- 0.7) \times 10^{10}$	0.4	2
K249C <sup>spin</sup> -S180C <sup>spin</sup>	$1.3 (+/-0.3) \times 10^{10}$	0.7	3.5
R131C	$1.1 (+/- 0.6) \times 10^9$	2.2	43

synthetic oligomers.<sup>[43, 44, 71]</sup> Recently, the DEER experiment has been used to probe structural rearrangements upon metal binding in the anthracis repressor, a DNA binding protein.<sup>[72]</sup>

The unprocessed time domain DEER signal for the R131C, K249C-S180C and S180C EcoRI complexes are shown in Figures 4,5, and 6, respectively. The baseline signal due to the intermolecular interaction is shown by a red dotted line in each figure. The modulation depth of the DEER signal varies for some of the samples despite the fact that we are only probing two spins in each sample. This is due to the fact that we used three different resonators to collect the entire series of experiments, and each resonator has a different probability for flipping spins with the pump pulse,  $P_b$ . Table 2 shows which resonator was used for each sample and the  $P_b$  determined by calibration with a standard biradical. Also, our initial experiments on the R131C samples were performed with the observer pulse positioned on the maximum of the spectra. We found that placing the pump pulse on the maximum of the spectrum gave us better sensitivity, so subsequent experiments with K249C-S180C and S180C complexes were performed in this way. The modulation depths,  $V_p$  and  $P_b$  can be used to solve for the number of spins,  $N$  in the complex using the equation,  $V_p=(1-P_b)^{N-1}$ .<sup>[50]</sup>

The R131C and S180C complexes have a reasonable modulation depth and when compared with the  $P_b$  for the resonator used, the number of spins in each complex is approximately two. However the same equation does not give a number of spins equal to four for K249C-S180C complexes as expected. Analysis of the modulation depth for the double mutant is more complicated due to the presence of nitroxides pairs that are  $\sim 30$  Å and  $\sim 60$  Å apart. As shown by Bode et al., when a sample contains a mixture of coupled spins, the modulation depth arises from contributions from all the spin pairs.<sup>[44]</sup>

## R131C

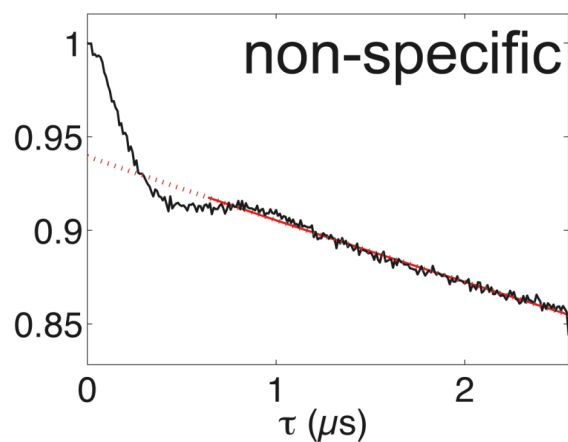
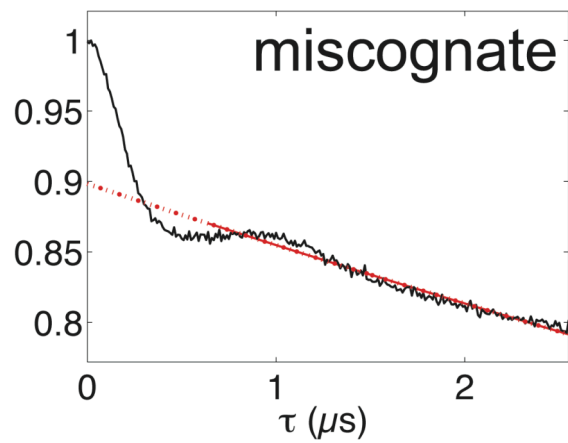
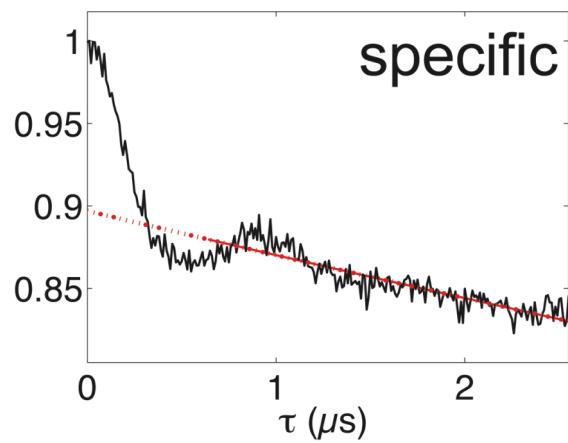


**Figure 2.4** Unprocessed time domain DEER signal for the R131C EcoRI complexes. The dotted red line in the time domain is the background correction.

## K249C-S180C

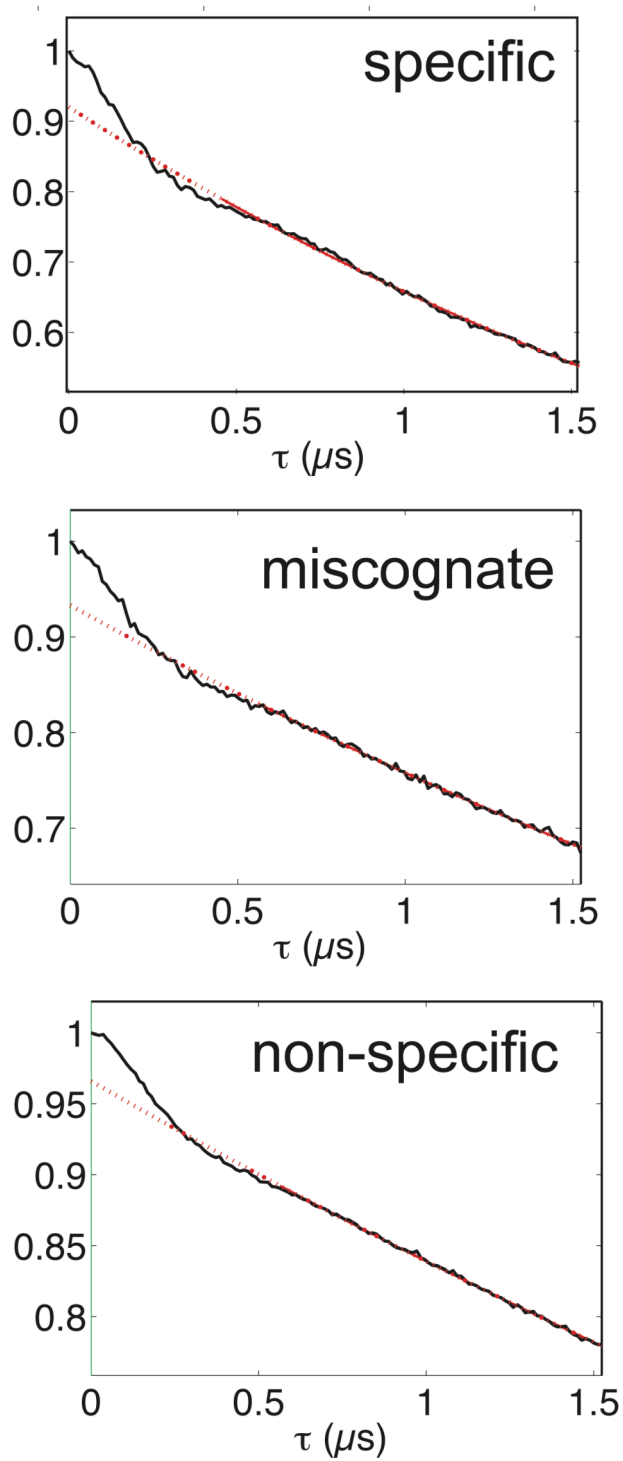
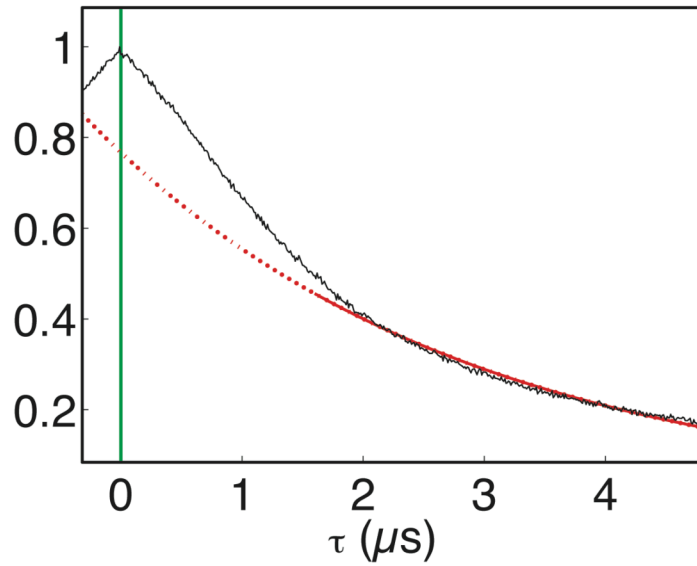
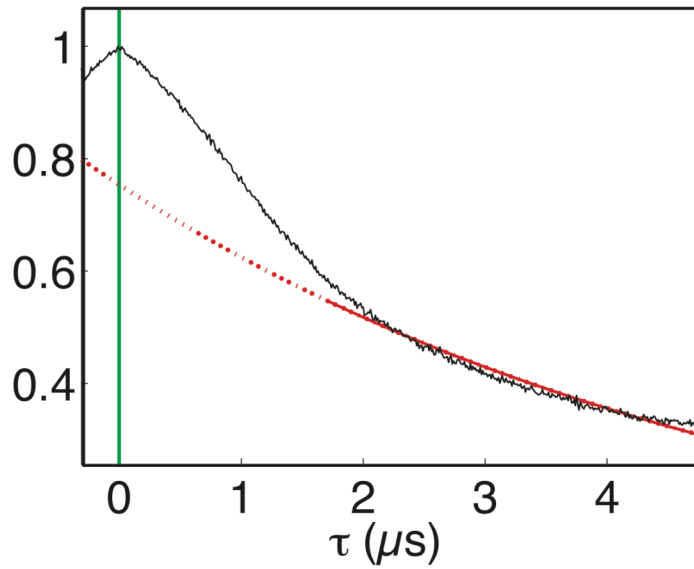


**Figure 2.5** Unprocessed time domain DEER signal for the K249C-S180C EcoRI complexes. The dotted red line is the background correction.

# S180C



specific



non-specific

**Figure 2.6** Unprocessed time domain DEER signal for the S180C EcoRI complexes. The dotted red line is the background correction, and the green line indicates the zero time.

**Table 2.2.** For each sample, the resonator used and the  $P_b$  for a given length of the pump pulse is given. \*The  $P_b$  values were determined by S. Pornsuwan and are reported in S. Pornsuwan, PhD thesis, University of Pittsburgh (Pittsburgh), 2007.

<b>Sample</b>	<b>Resonator</b>	<b>Length of pump pulse (ns)</b>	<b><math>P_b</math> *</b>
<b>R131C specific</b>	<b>MS3</b>	<b>48</b>	<b>0.12</b>
<b>R131C miscog</b>	<b>MS3</b>	<b>48</b>	<b>0.12</b>
<b>R131C NS</b>	<b>MS2</b>	<b>48</b>	<b>0.07</b>
<b>K249C-S180C specific</b>	<b>MS3</b>	<b>32</b>	<b>0.13</b>
<b>K249C-S180C miscog</b>	<b>MS3</b>	<b>32</b>	<b>0.13</b>
<b>K249C-S180C NS</b>	<b>MS3</b>	<b>48</b>	<b>0.12</b>
<b>S180C specific</b>	<b>MD5</b>	<b>32</b>	<b>0.26</b>
<b>S180C NS</b>	<b>MD5</b>	<b>32</b>	<b>0.26</b>

Specifically, a scaling factor must be used which takes into account the transverse relaxation of each of the dipolar couplings.

The background corrected DEER signal for the R131C mutant in each complex is shown in Figure 7a. The time domain signals were inverted to obtain the distance distribution functions, using a Tikhonov regularization method in the DEERAnalysis2006 program.<sup>[73]</sup> The resulting distance distribution functions are shown in Figure 7b. The most probable distances between the spin labels for the R131C EcoRI specific, miscognate, and non-specific complexes are 35 Å, 36 Å and 35 Å, respectively. The R131 C<sub>β</sub>-C<sub>β</sub> distance in the crystal structure of the specific complex is 32 Å.<sup>[57, 58]</sup> The interspin distance measured by ESR is expected to differ because of the added length of the spin label. Within the length of the linker, the ESR distances are consistent with the crystal structure. The R131C specific complex distance distribution has an unexpected small peak at ~55 Å. It is likely that the peak is an artifact of the Tikhonov regularization procedure. In order to test this, we suppressed the 55 Å peak. Figure 8a and b show the original time domain data and distance distribution function with no suppression. Figure 8c shows the fit of the time domain data when the 55 Å peak is suppressed (Figure 8d). The two fits are negligibly different, so we conclude that the peak is an artifact.

Distance measurements were performed on the S180C EcoRI mutant in the specific and non-specific complexes, as shown in Figure 9a. As with R131C, distance distributions were obtained by the Tikhonov regularization (Fig. 9b). Residue 180 lies in the outer arm of the protein complex, and the inter-spin distance is quite large. The most probable distance for the S180C mutant in the specific and non-specific complexes is 64 Å. The 180 C<sub>β</sub>-C<sub>β</sub> distance from the crystal structure of the specific complex is 59 Å. Again, 64Å is in reasonable agreement with

the crystal structure taking into account the length of the nitroxide linker. To enable measurement of such a large distance, a large volume of S180C in 30% deuterated glycerol, 65% deuterated water, and 5% protonated water was used, and the temperature was lowered to 40 K. With the enhanced signal and increased phase memory time (3  $\mu$ s), a sufficiently long dipolar evolution time could be collected.

The time domain signal for the specific, miscognate and non-specific complexes of the K249C-S180C mutant protein are shown in Figure 10a. The most probable experimental distance was 33 Å in all cases (Figure 10b). In principle, multiple distances corresponding to S180C-S180C, K249C-K249C, and S180C-K249C distances are anticipated for the K249-S180C double mutant. The corresponding C $\beta$ -C $\beta$  distances in the specific complex crystal structure are 27 Å (S180C-K249C intra-monomer), 59 Å (S180C-S180C), 60 Å (K249-K249), and 57 Å (S180-K249 inter-monomer).<sup>[57, 58]</sup> It is likely that the larger distances were not detected in this series of experiments given that only  $\sim$ 1.5  $\mu$ s of the data could be collected due to short phase memory times. The 33 Å peak for the double mutant can thus be assigned to the S180C-K249C intra-monomer distance.

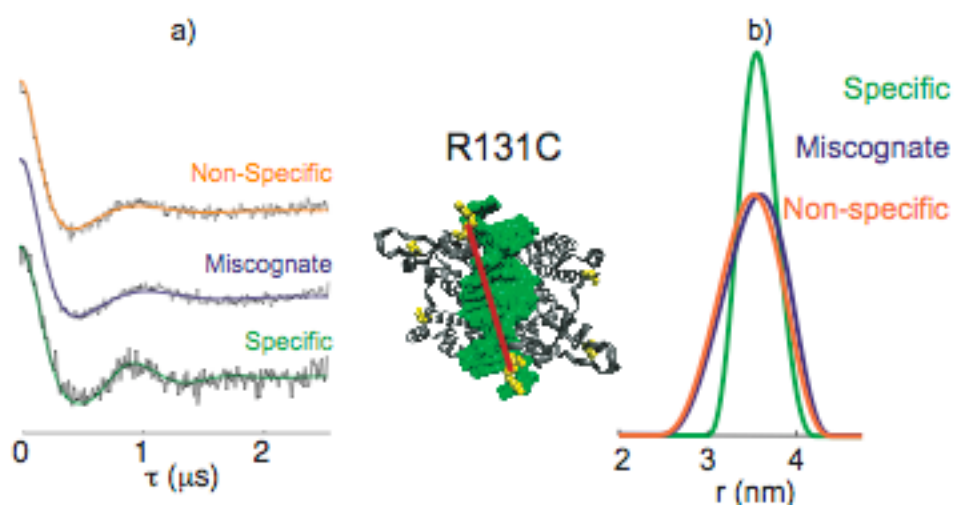


**Figure 2.7** (a) DEER data for R131C specific, miscognate and non-specific complexes. Simulated traces based on the distance distributions are overlaid on the experimental signal. (b) Normalized distance distribution functions. Red lines in the crystal structure indicate distance measured.

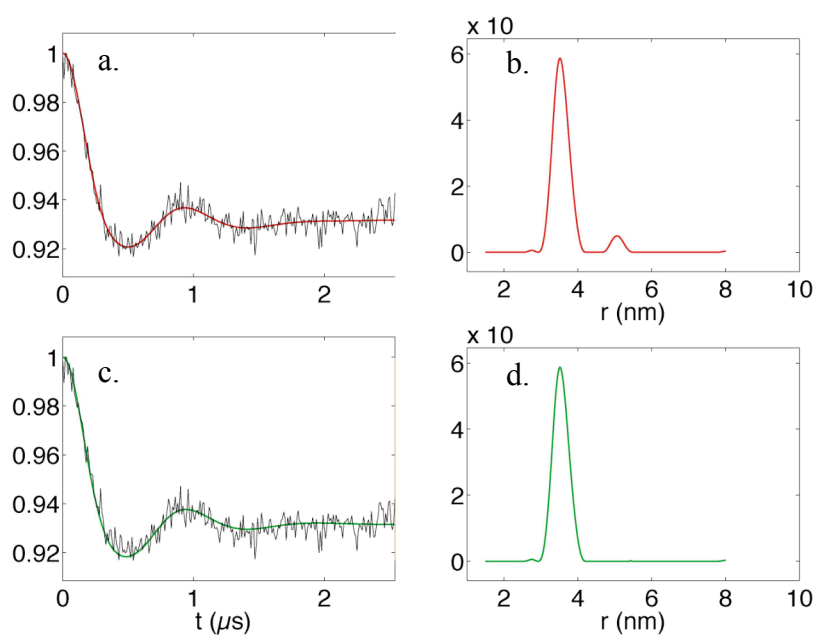


**Figure 2.8** The time domain signal for the R131C specific complex with the simulated signal overlaid in red (a) and the resulting distance distribution function (b). Time domain signal and simulated signal overlaid in green (c) for the suppression of the 55 Å peak in the distance distribution function (d).

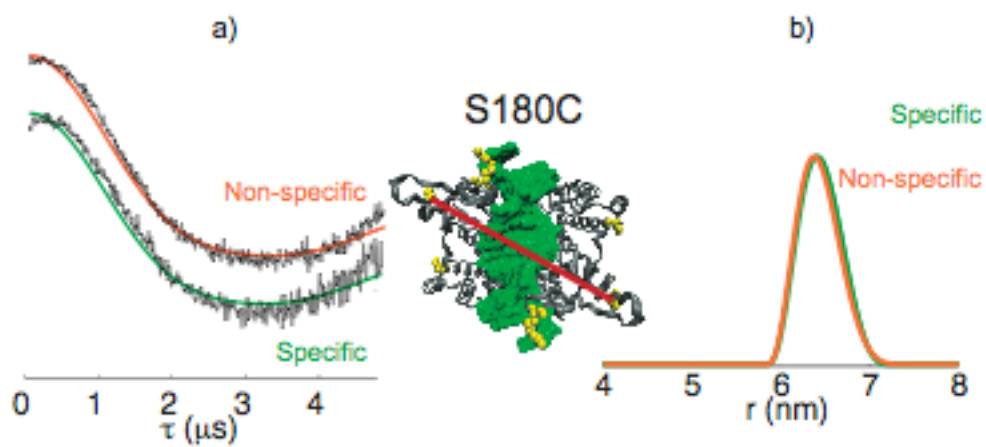


**Figure 2.9** (a) DEER data for S180C specific and non-specific complexes. Simulated traces based on the distance distributions are overlaid on the experimental signal. (b) Normalized distance distribution functions. Red lines in the crystal structure indicate distance measured.

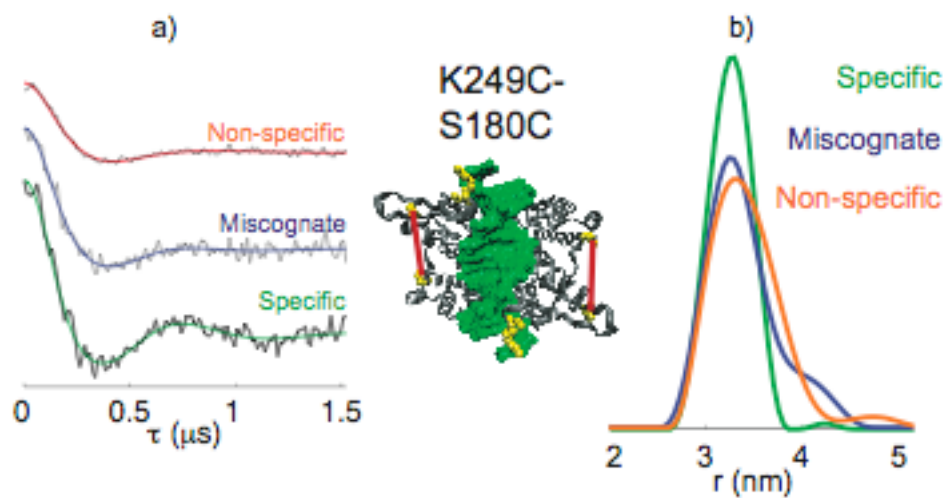


**Figure 2.10** (a) DEER data for the double mutant, K249C-S180C specific, miscognate and non-specific complexes. Simulated traces based on the distance distributions are overlaid on the experimental signal. (b) Normalized distance distribution functions. Red lines in the crystal structure indicate distance measured.

Strikingly, the experimental point-to-point distances are very similar for specific, and non-cognate (i.e. miscognate and non-specific) EcoRI-DNA complexes. The data show preservation of the distances between the inner arms (R131C data), outer arms (S180C data), and from the outer arm (S180C) to a fixed reference point (K249C) in the main domain. For both the R131C and K249C-S180C mutant proteins, the distance distribution is narrower for the specific complex than for the corresponding non-cognate complexes. This might indicate a greater flexibility of the arms in the EcoRI complex with non-cognate DNA. Further ESR experiments that probe dynamics are underway to confirm this hypothesis. In addition, the distributions for both the R131C inter-arm distance and the K249C-S180C distance show asymmetries in the non-cognate complexes. However, it is unclear if this represents an asymmetric set of accessible conformations of the arms or different orientations accessible to the spin labels.

Taken together the data suggest that on average the EcoRI arms envelop the DNA and are similarly oriented in non-cognate and specific DNA complexes. This implies that the DNA in the specific and non-specific complexes occupies roughly the same binding cleft of the EcoRI dimer. In addition, slopes of the salt dependence for formation of specific and non-specific complexes are the same ( $d \log K_A / d \log [\text{NaCl}] \sim -11$ )<sup>[74]</sup> and are consistent with the number of Coulombic interactions observed in the specific complex. This provides additional strong evidence that the arms enfold the DNA in the non-specific complex. This enfolding may contribute to processivity as the protein slides along non-specific DNA<sup>[59, 60, 75, 76]</sup> to locate its specific recognition site. In other words, the EcoRI appears to remain bound to the template DNA as it searches for its specific site instead of hopping across strands. Our results on a DNA-protein complex by pulsed ESR establish a methodology that can measure the solution structure and range of

conformational states for complexes with different classes of DNA sites for which there is little or no prior structural information.

**Acknowledgements.** This work was supported by an NSF CAREER grant (MCB 0346898) to S.S. and an NIH MERIT 5R37M029207 grant to L.J.-J.

### **3.0 MEASUREMENT OF INTER-SUBUNIT SEPARATIONS IN THE M3 DOMAIN OF A LIGAND GATED ION CHANNEL BY ELECTRON SPIN RESONANCE**

#### **3.1 ABSTRACT**

In this chapter, we apply site-directed spin labeling (SDSL) and electron spin resonance (ESR) to the case of the human  $\alpha 1$  glycine receptor (GlyR), a member of the ligand-gated ion channel superfamily. We show that it is possible to react cysteines with thiol-reactive spin labels even in the transmembrane domain of the  $\sim 250$  kDa GlyR channels. We generated a series of cysteine mutants in the M3 transmembrane domain of the homopentameric  $\alpha 1$  GlyR the channel. Using DEER-ESR, we show that on average 1-2 cysteines in each channel were chemically modified. Preliminary distance measurements indicate that two sets of inter-subunit distances were measured, as expected from the pentagonal symmetry of the channel. These experiments demonstrate the applicability of ESR distance measurements on ligand-gated ion channels, which may provide us with constraints to quantitate subunit packings at the spin-labeled site. Systematic state-dependent nitroxide-scanning experiments of the GlyR in conjunction with distance measurements will be the key determinant in developing a detailed understanding of conformational changes that underlie the function of nicotinicoid receptors.

## 3.2 INTRODUCTION

Over the last decade, ESR has been established as an attractive method for structural and dynamical measurements of membrane proteins. The success of ESR for protein research is based on the concerted development of approaches for site-directed spin labeling (SDSL) of proteins,<sup>[77-79]</sup> methods for extracting motional and spin relaxation rates from ESR spectra,<sup>[80-82]</sup> and systematic procedures for relating motional and relaxation rates to biophysical information such as secondary structures, tertiary interactions, and depths of immersion at the labeled sites.<sup>[78, 79, 83]</sup> In pioneering papers, Hubbell and coworkers have used ESR to determine the secondary structures, tertiary interactions and conformational changes of bacteriorhodopsin and the large amplitude domain motions of the T4 lysozyme.<sup>[79]</sup> These experiments provided a foundation for the routine investigation of membrane proteins by SDSL and ESR.

Structural features and structural changes in a variety of membrane protein complexes have been characterized by ESR. Some notable examples include the use of ESR to examine signaling events in the membrane transport protein, BtuB,<sup>[84]</sup> as well as probe the order-to-disorder transition of the Ton box of several transporters.<sup>[85]</sup> Additionally, ESR has been used to quantify hemifusion processes in the SNARE assembly,<sup>[86]</sup> the partial backbone structure of the Na<sup>+</sup>/proline transporter,<sup>[87]</sup> and large amplitude conformational motions of the MsbA transporter.<sup>[88]</sup> However, one of the most exciting areas of advancement in SDSL and ESR has been in ion channels. Freed and coworkers have used ESR to investigate the effect of lipid composition and phase on spin labeled gramicidin channels.<sup>[89]</sup> Perozo and coworkers have determined gating mechanisms and structural features of the open state of a potassium channel, KcsA,<sup>[90-92]</sup> and a mechanoselective ion channel, MscL,<sup>[93]</sup> by systematic spin labeling of entire domains. They also analyzed the accessibility of spin labeled residues in the highly controversial

voltage-sensor domain of the KvAP potassium channel.<sup>[83]</sup> Through experiments corroborated by Gross and coworkers,<sup>[94]</sup> Perozo provided key data, which underscores the importance of a native lipid environment in the structural analysis of KvAP.<sup>[95]</sup>

Recent developments in ESR now permit the measurement of the weak electron-electron dipolar interaction between two spin labels<sup>[33-43]</sup> in order to determine the interspin distances in the ~8-70 Å range. Methods also exist for inverting the experimental data to obtain the full distance distribution function.<sup>[47, 73]</sup> Access to this range of distances is crucial for measuring global folding patterns and large amplitude domain motions in membrane proteins. In the analysis of membrane proteins, the extraction of multiple distances originating from multiple spin interactions in the experimental data is also of critical importance as so many membrane proteins are oligomeric complexes.

In a series of papers, Jeschke and coworkers have demonstrated the utility of pulsed ESR distance methods, and in particular the four-pulse Double Electron-Electron Resonance (DEER) ESR experiment, to the case of oligomeric membrane proteins with multiple spin interactions. Four-pulse DEER-ESR<sup>[38]</sup> was used to quantify pH-dependent conformational changes and the extent of oligomerization for the NhaA Na<sup>+</sup>/H<sup>+</sup> antiporter,<sup>[96]</sup> and conformational motions in a trimeric light-harvesting chlorophyll *a/b* complex.<sup>[97]</sup> Although single distances were expected from the trimeric symmetry, site-specific structural constraints on two conformations due to the simultaneous coexistence of both conformations could be measured. Multiple distance constraints were also measured in the KvAP channel,<sup>[94]</sup> the lactose permease,<sup>[66]</sup> the ribonucleotide reductase,<sup>[67]</sup> double stranded DNA,<sup>[98, 99]</sup> and oligomeric microbial peptides.<sup>[49, 50, 100]</sup> These experiments elegantly show the utility of exploiting multiple spin interactions

originating either by symmetry or conformational switching to measure structural and mechanistic constraints.

In this work, we generalize the approach of symmetry related spin labeling to the measurement of inter-subunit separations in a mammalian pentameric membrane protein. We specifically focus on the glycine receptor (GlyR), an approximately 250 kDa chloride ion channel essential for electrical signaling in synapses. The GlyR is a member of the nicotinicoid superfamily of receptors, a sub-class of proteins that form ligand-gated ion channels in cellular membranes. Despite the success of SDSL and ESR on a variety of membrane protein complexes, it is not immediately obvious that the glycine receptor will be amenable to the technique. Unlike most of the membrane proteins that have been investigated by ESR, the glycine receptor is a mammalian protein, which cannot be expressed in bacteria. The baculovirus-driven overexpression of human  $\alpha 1$  GlyR in infected insect cells, although relatively high for a membrane protein ( $\sim 1$  mg of purified, reconstituted receptor per liter),<sup>[101, 102]</sup> is still at the limit of detection for pulsed ESR. Also, many authors spin label under conditions that could potentially denature GlyR. Residues in the MscL, BtuB and LHCIIB membrane protein complexes were spin labeled while the protein was detergent solubilized at room temperature.<sup>[28, 84, 97]</sup> In some cases, proteins have been partially unfolded to increase the accessibility of a residue to the spin label. Thomas and coworkers showed that the reactivity of the cysteines in phospholamban dramatically increased when the protein was reversibly denatured by guanidine HCl.<sup>[103]</sup> There are a number of membrane proteins that spontaneously refold after denaturation. However, it is not expected that GlyR will refold with ease, given the complexity of its pentameric assembly and the difficulty of reconstituting detergent-solubilized GlyR.

Figure 1 illustrates some structural features of nicotinicoid receptors. Typically, these receptors assemble as heteropentamers, and each subunit contains a large extracellular ligand-binding domain, a transmembrane domain, and a smaller intracellular domain. The transmembrane domain on each subunit contains four membrane-spanning segments, labeled M1-M4, and the amphiphilic  $\alpha$ -helical M2 segment of each subunit lines the conducting central pore.<sup>[104]</sup> These channels transiently permit the flux of anions or cations across the membranes in response to their respective neurotransmitter agonist. In the case of the inhibitory GlyR, glycine gates anion flow across the cell membrane.<sup>[105, 106]</sup>

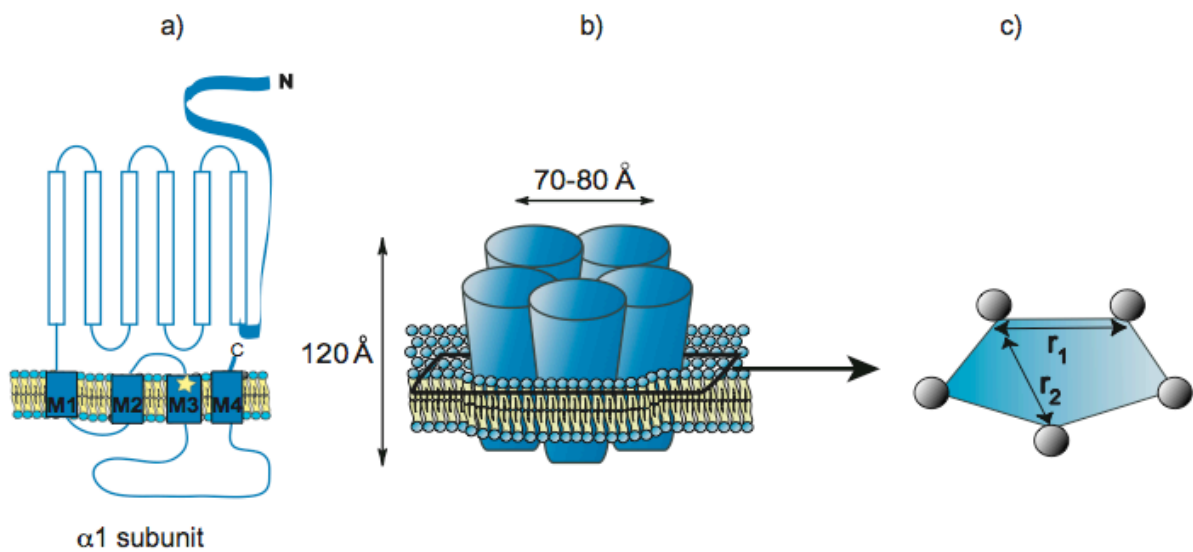


**Figure 3.1** (a) The structure of the  $\alpha 1$  subunit of GlyR is illustrated. Each subunit consists of extracellular domain, a transmembrane domain and an intracellular loop. The star indicates the third transmembrane segment, M3. (b) Five subunits oligomerize to form a central channel through the membrane in the 250 kDa GlyR (c) Due to the pentagonal symmetry of the channel, spin labeled single cysteine mutants of GlyR yields five spin labeled positions and two unique distances,  $r_1$  and  $r_2$ .

Electron microscopic studies on tubular arrays of nicotinic acetylcholine receptor (nAChR)<sup>[107-109]</sup> and on two-dimensional crystalline arrays of GABA receptor<sup>[110]</sup> indicate that nicotinicoid receptors are approximately 120 Å long and have a diameter of 70-80 Å. The extracellular domain consists of a funnel protruding ~60 Å from the membrane surface,<sup>[111]</sup> and contains the binding site for agonist and competitors at the subunit interfaces. The modular nature of the receptors and the general conservation of the gating mechanisms across the nicotinicoid family is illustrated by the activity of chimeric receptors in which the ligand-binding domain of the nAChR in combination with the ion pore domain of the GlyR formed acetylcholine-gated channels with conductance properties of GlyR channels.<sup>[112]</sup>

Recent electron cryomicroscopic (cryo-EM) studies have resolved the structure of nAChR to ~ 4 Å.<sup>[113]</sup> Additionally, the structure of a prokaryotic ligand-gated ion channel, which exhibits high sequence homology to the nAChR, was resolved to ~3.3 Å.<sup>[114]</sup> Taken together, these structures provide a template for research that probes the atomic level details of ion solvation, permeation, receptor allostery, anesthetic binding, and importantly, gating of nicotinicoid receptors. Given the recent methodological advances in ESR, we explore the use of site-directed spin labeling and pulsed ESR to obtain distance constraints between segments of the GlyR, in order to ultimately understand these mechanisms at an amino-acid level.

In this work, we demonstrate the feasibility of site-directed spin labeling in the homomeric membrane protein. We show that cysteines in the transmembrane segments are accessible to the spin label even when the channel is reconstituted in lipid vesicles. Seven cysteine mutants were generated at the top of the M3 domain. The M3 domain is an area of interest in the GlyR due to its proximity to the proposed anesthetic binding pocket,<sup>[115]</sup> and it is believed to undergo conformational changes as the channel cycles through the open, closed and

desensitized states.<sup>[116]</sup> Previous biochemical studies have suggested that some residues at the top of M3 are inaccessible to MTS reagents, and indeed the solvent accessibility of this region is unknown.<sup>[117]</sup> Our data suggests that residues 286-292 of the GlyR are accessible to MTS reagents, although at sub-stoichiometric amounts. We also present preliminary distance measurements on the spin labeled mutants and show that distance constraints may be obtained on homomeric human  $\alpha 1$  GlyR channels reconstituted in lipid vesicles using pulsed ESR in order to measure subunit packings at the spin labeled site. These results foreshadow subsequent measurements that exploit the developed methodology to systematically label targeted residues of the GlyR in order to examine the structure and dynamics of this physiologically important receptor.

### 3.3 MATERIALS AND METHODS

- **Mutagenesis, expression, and purification of GlyR mutants**

A double mutant, denoted C290-GlyR, was constructed by sequential site-directed mutagenesis of the  $\alpha 1$  GlyR in a mammalian expression vector (pCDNA3) such that a single reactive cysteine at position 290 was retained in each  $\alpha 1$  subunit. In this mutant, the free cysteines in the wild type GlyR at positions 41 and 345 were replaced with serine. The C290-GlyR gene was subcloned into the pFastBac plasmid (Invitrogen) and subsequently was used to make a cys-null GlyR gene. The Quick Change Site Directed Mutagenesis Kit (Stratagene) was used to replace the cysteine at position 290 with an alanine leaving no free cysteines. The cys-null GlyR gene in pFastBac was then used to generate single cysteine mutants in positions 286-289, 291, and 292. Baculovirus directing the synthesis of each of the single cysteine GlyR

mutant genes were produced by following standard protocols for virus production, purification, amplification and titration as described by the manufacturer (Invitrogen). Functional, recombinant mutant GlyR was purified and reconstituted as described previously.<sup>[101]</sup> Briefly, Sf9 cells were grown in spinner flasks (at ~50 rpm) at 27°C in Grace's Insect Media supplemented with 10% Fetal Bovine Serum. 800 mL of Sf9 cells at an initial density of  $\sim 1 \times 10^6$  cells/ml were infected with virus at a multiplicity of infection (MOI) of  $> 5$ . Three days post-infection, the cells were collected by centrifugation at  $1000 \times g$ . All membrane proteins were enriched from the whole cell extract by lysis and centrifugation and membranes were washed with high salt buffer to remove peripheral membrane proteins. Integral membrane proteins were solubilized in buffer containing digitonin, deoxycholate, and egg lecithin lipids. The GlyR mutants in mixed micelles were affinity purified by binding to 2-aminostrychnine agarose and eluted with buffer containing 200 mM glycine, pH 7.4. This affinity chromatography step wherein the solubilized receptor binds to an aminostrychnine matrix (strychnine is a competitive antagonist with nM affinity to GlyR) and is competed off with excess glycine naturally screens for functional channels, as indicated by mass flux assays.<sup>[102]</sup> It is therefore expected that no monomers or other oligomeric forms of GlyR are present after reconstitution into vesicles. Purified GlyR mutants were reconstituted in egg lecithin lipid vesicles at  $\sim 10,000:1$  lipid:channel molar ratio by dialysis in a 10,000 MWCO Slide-A-Lyzer cassette (Pierce) in 25 mM potassium phosphate buffer at pH 7.4. The protein was dialyzed against buffer containing 1 mM DTT until the last buffer change in order to ensure that the free cysteines remained reduced. Protein concentrations were determined by a modified Lowry assay.

- **Spin labeling**

The spin label (1-Oxyl-2,2,5,5-tetramethyl-3-pyrroline-3-methyl) Methanethiosulfonate (MTSSL) was purchased from Toronto Research Chemicals Inc (Ontario, Canada). MTSSL was dissolved in acetonitrile, and a 50 molar excess of label was reacted with reconstituted GlyR mutant protein in the presence of 0.030 M glycine for 4 hours and again overnight each at 4 °C with nutation. Unbound label was removed by dialysis in a 10,000 MWCO Slide-A-Lyzer cassette (Pierce) in 25 mM potassium phosphate buffer at pH 7.4. The reconstituted spin labeled protein was collected by ultracentrifugation at  $150,000 \times g$  for 60 minutes. Approximately 100  $\mu\text{L}$  of sample was loaded into a 5 mm OD quartz tube with 20% glycerol added as a cryoprotectant. Before ESR experiments, the sample was quick frozen in liquid nitrogen cooled propane.

- **ESR Experiments**

The DEER experiment was performed on all seven mutants of the glycine receptor in order to extract the inter-residue distances. The ESR experiments were performed at 80 K using a Bruker EleXsys E580 X-band ESR spectrometer equipped with a Bruker ER 4118X-MD-5 X-band dielectric resonator. The temperature was stabilized using an Oxford IT C605 temperature controller and ER 4118 CF gas flow cryostat. An ASE TWTA was used to provide output power of 1 kW. The four pulse DEER sequence,  $(\pi/2)_{\nu,a}-\tau_1-(\pi)_{\nu,a}-t'-(\pi)_{\nu,b}-\tau_1+\tau_2-t'-(\pi)_{\nu,a}-\tau_2$ -echo, was used with a two-step phase cycle for baseline correction. The  $\pi/2$  and  $\pi$  pulses were 16 and 32 ns respectively,  $\tau_1$  was 200 ns, and  $\tau_2$  was chosen to be 1200 ns based on the phase memory time ( $T_m$ ) of each sample. The pump pulse began either 32 or 64 ns before the maximum of the echo in order to accurately determine the zero time of the experiment. The pump pulse frequency was placed at the maximum of the nitroxide spectrum and the observer pulse frequency was placed

64-67 MHz higher at the local maximum of the low field component of the nitroxide spectrum. The inter pulse delay,  $t'$ , was incremented 8 ns, and the integrated echo intensity was collected for 128 points. The total data acquisition times were 15-44 hours, depending on the signal to noise of the sample, and the experimental error in the distances reported is ~10 %.

- **Data Analysis**

The time domain DEER signals were analyzed using the DeerAnalysis2006 program,[46] and the distance distributions were obtained. A background correction was performed in order to separate the intermolecular interactions from the intramolecular interactions by fitting approximately the last 80% of the data points to an exponential function assuming a homogeneous three-dimensional distribution. To the background corrected signal, the Tikhonov regularization method was used to generate the distance distribution functions. The L-curve criterion was used to find the best regularization parameter, and a value of 100 was appropriate for all samples except for the C289-GlyR mutant, for which a value of 10 was used.

### 3.4 RESULTS AND DISCUSSION

While the GlyR is naturally a heteropentamer, we focused on the homomeric  $\alpha 1$  GlyR which retains the activity of the wild type GlyR when overexpressed in insect cells.<sup>44</sup> Spectroscopic measurements on the homomeric  $\alpha 1$  GlyR channels decrease the complexity of analyses by eliminating subunit heterogeneity, thereby permitting the use of symmetry elements. Each subunit in the wild type  $\alpha 1$  GlyR contains seven cysteines of which four are engaged in disulfide bonds essential for activity (C138-C152, C198-C209). The free cysteines with reactive thiols that may potentially be labeled are in positions C41, C290, and C345. Thus complete spin labeling of the  $\alpha 1$  GlyR with MTSSL could potentially yield a pentameric receptor with 15 labels.

In order to reduce the complexity of the system, a series of mutants with only one free Cys per subunit (C286-C292) and mutations corresponding to C41S and C345S were overexpressed and purified from insect cells and functionally reconstituted into lipid vesicles. These mutations were made without any apparent change in the receptor activity as the affinity chromatography step during purification of GlyR only yields functional channels. Additionally, the triple mutant in which all three free thiols are mutagenized is fully functional, though state-dependent labeling of C290 with MTS reagents does inhibit receptor activity.<sup>[117]</sup> The residues C286-C292 are positioned in the transmembrane M3 helix, which is proposed to begin at residue 285.<sup>[118, 119]</sup> These residues are in close proximity to the proposed anesthetic binding pocket comprised of residues from M3 and its neighboring TM segments.<sup>[118, 119]</sup> Experiments on other nicotinicoid receptors showed that the M3 region had increased mobility and became relatively accessible to modification by aqueous agents only in the presence of agonist.<sup>[120-123]</sup> Thus the free

cysteines at the sites C286-C292 were spin labeled by incubating the receptor with saturating levels of MTSSL in the presence of glycine for a prolonged period of time. As expected, no detectable ESR signal was observed when the reconstituted receptor was labeled in the absence of glycine.

The DEER signal was collected for each of the seven mutants of GlyR, and the time domain signals are shown in Figures 2 and 3. The DEER signal can be used to calculate the number of coupled spins in each protein complex. The modulation depth of the background corrected signal is related to the number of coupled spins by

$$V_p = (1 - p_b)^{n-1}, \quad [2]$$

where  $V_p$  is the limiting value of the intramolecular component of the DEER signal,  $p_b$  is the fraction of spins excited by the pump pulse and  $n$  is the number of coupled spins. We determined that each mutant had  $\sim 1.3$  coupled spins per channel. It should be noted that there were considerable difficulties in finding an appropriate spin labeling technique for GlyR. Appendix B gives details on the issues associated with spin labeling this system, including maximizing the reactivity of the cysteines while minimizing association of the spin label with the charged lipid head groups.

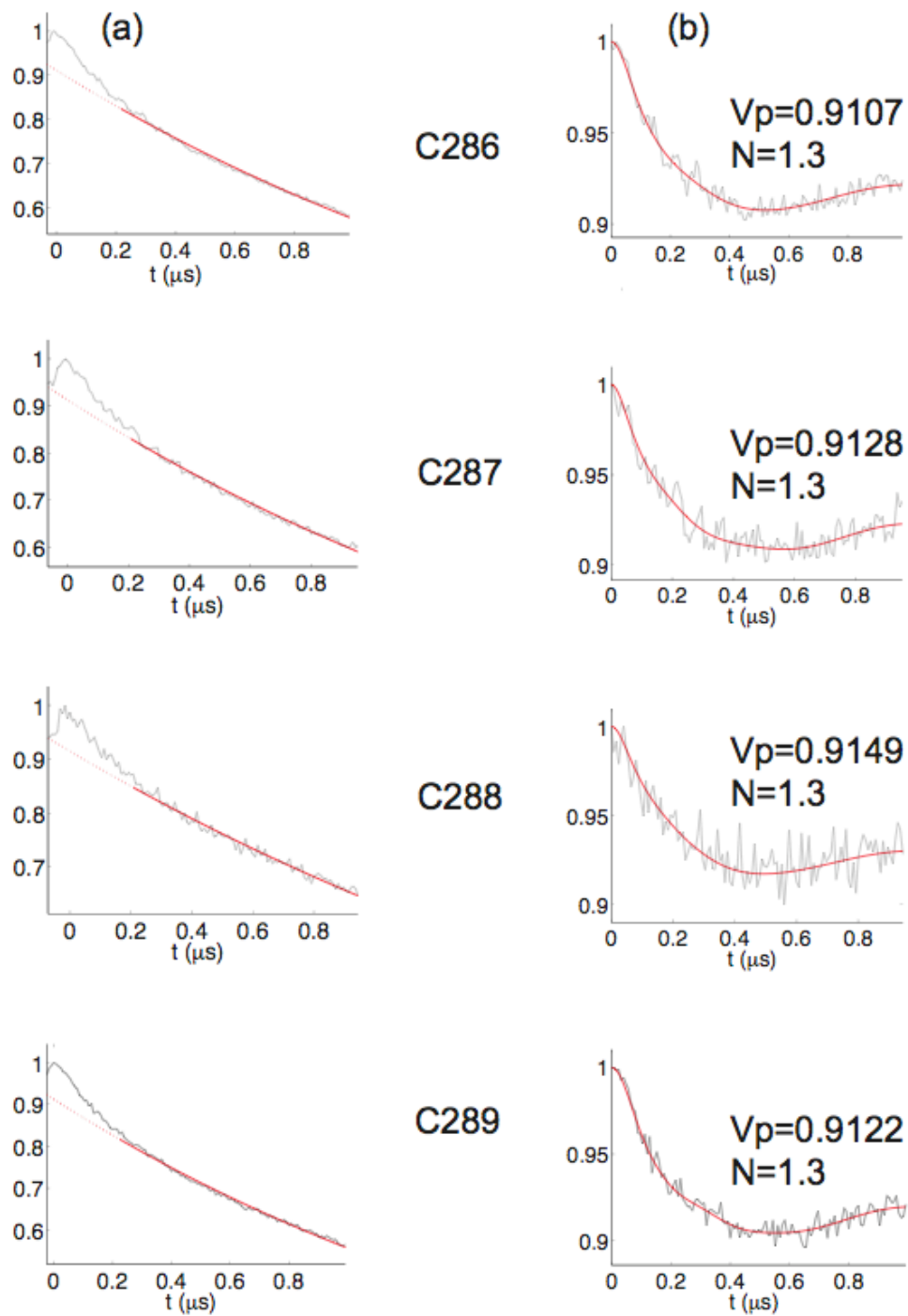


**Figure 3.2** (a) Unprocessed time domain DEER signal for C286-C289 mutants. The red line was used to divide out the contribution from the intermolecular interaction. (b) The background corrected  $V_{\text{intra}}$  DEER signal. The limiting  $V_{\text{intra}}$  value,  $V_p$  is given for each mutant as well as the number of coupled spins,  $N$ .

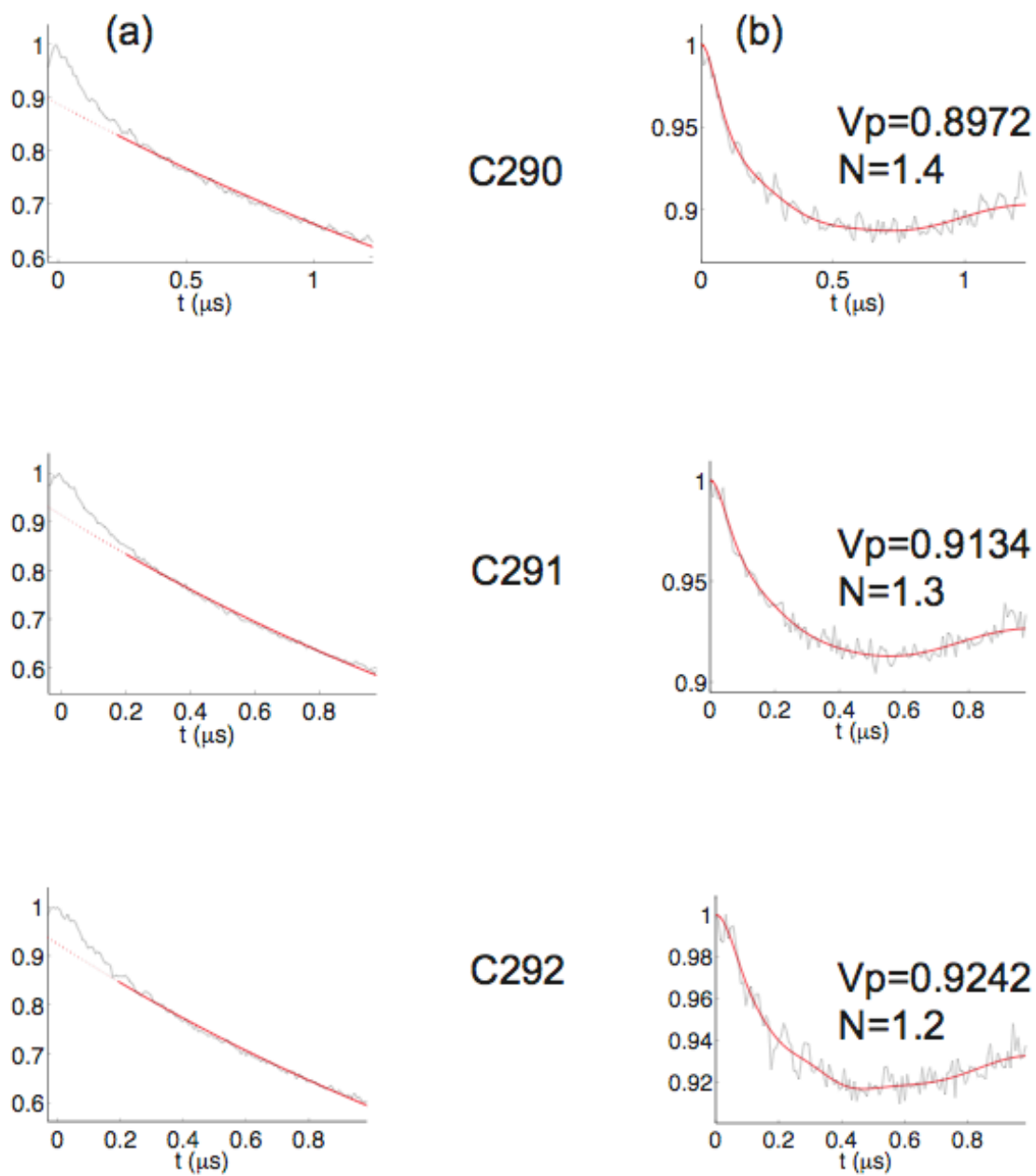


**Figure 3.3** (a) Unprocessed time domain DEER signal for C290-C292 mutants. The red line was used to divide out the contribution from the intermolecular interaction. (b) The background corrected  $V_{\text{intra}}$  DEER signal. The limiting  $V_{\text{intra}}$  value,  $V_p$  is given for each mutant as well as the number of coupled spins,  $N$ .

In addition to providing the number of coupled spins per molecule, the DEER experiment can be used to extract the inter-spin distances, as shown in Figure 4. In these experiments, the electron-electron dipolar interaction leads to a modulation of the time domain signal. For the case of an isolated spin-pair, the modulation leads to a peak at a frequency,  $\nu$  of:

$$\nu = \frac{\mu_0 g^2 \beta^2}{4 \pi \hbar r^3} (3 \cos^2 \theta - 1) \quad [1]$$

where  $r$  is the distance between the two spins,  $\theta$  is the angle between the static magnetic field and the interspin vector,  $\beta$  is the Bohr magneton,  $\hbar$  is Planck's constant,  $\mu_0$  is the magnetic permeability of vacuum and  $g$  is the  $g$ -factor of the MTSSL label. The time domain DEER signals for each mutant C286-C292 were inverted in order to obtain the distance distribution functions using a Tikhonov regularization method from the DEERAnalysis2006 program.<sup>[46]</sup> The distance distributions are shown in Figure 4c. Within experimental error, each mutant has two unique distances with an average of 25 and 36 Å. Two sets of distances are expected due to the pentagonal symmetry of the channel (Fig. 1c). We assign the shorter distance,  $r_1$ , to the separation between adjacent subunits and the longer distance,  $r_2$ , to the separation between subunits arranged one subunit apart.

Since the modulation depth of the time domain DEER signal indicated that only 1-2 cysteines per channel were modified by the MTSSL, we considered the possibility of preferential labeling. We measured the ratio of the area under the curves of the two components,  $P(r_2)/P(r_1)$ , and those values are shown in Figure 4c. In accordance with the pentagonal symmetry of the channel, if all five cysteines were labeled in each channel, the ratio  $P(r_2)/P(r_1)$  would be equal to 1, since there is equal probability for both distances. For each of the mutants, the ratio is greater than one, suggesting that labeling of cysteines on non-adjacent subunits was slightly favored. It

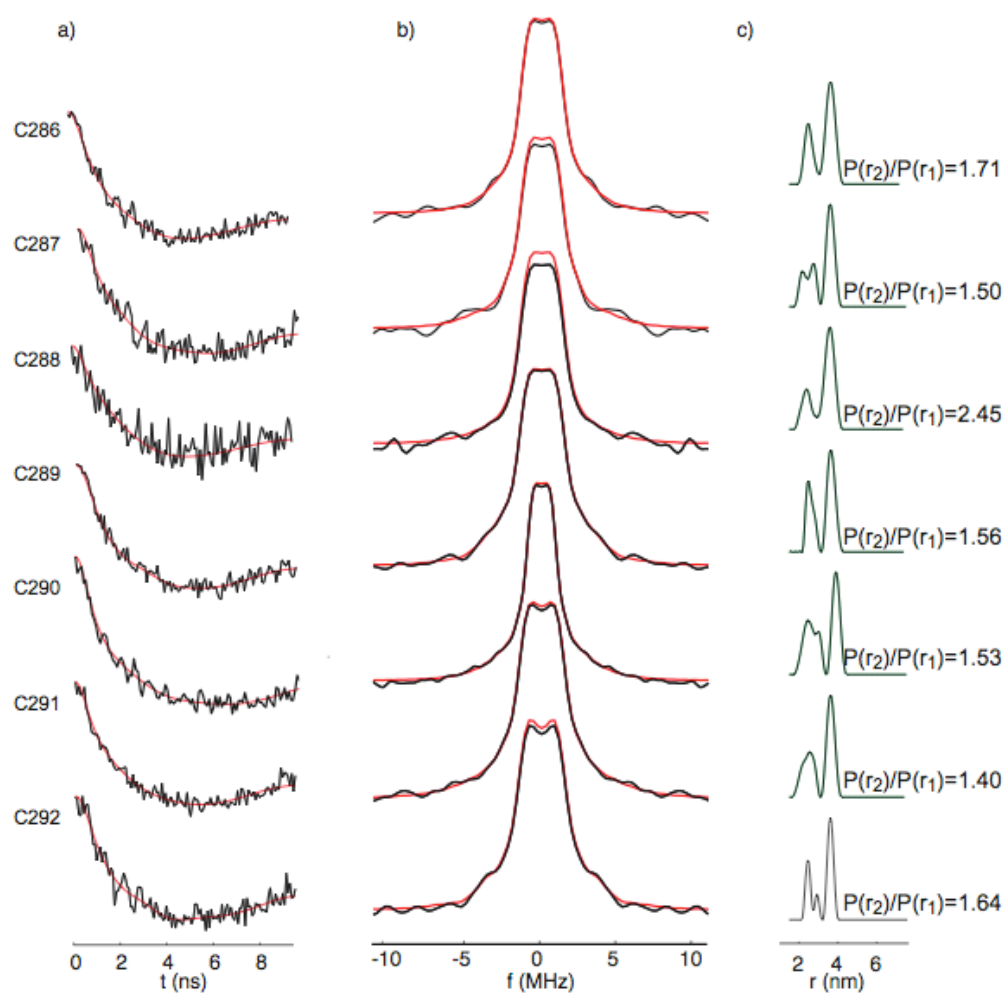


**Figure 3.4.** a) The DEER-ESR time and b) frequency domain signals for GlyR mutants C286-C292. Simulated traces based on the c) distance distribution functions generated in DEERAnalysis2006 are overlaid in red. Two distances were measured for each sample averaging approximately 25 and 36 Å.

is possible that the remaining cysteines did not react with the MTSSL because of a decreased accessibility. Future experiments will be performed in order to establish the reactivity of transmembrane cysteines. The results may indicate that allosteric effects limit the number of cysteines that are available to react with the nitroxide label.

Although the preliminary nature of our data precludes us from definitively characterizing the orientation of the M3 domain, within experimental uncertainties, the two distances are in reasonable agreement with the expected pentagonal symmetry. Additionally, the distances between labels incorporated at C290 may be compared to the distances between  $\beta$ -carbons of the homologous residues in the structure of nAChR.<sup>[113]</sup> The two distances between homologous residues of nAChR are 24.5 and 39 Å, and our data are consistent with this model taking into account the addition of the MTSSL linker. One may also compare the results in terms of the pore radius of the pentagons created by the symmetrically arranged spin labeled residue and the homologous residue of nAChR. The pore radius of the C290-GlyR is ~17 Å which is in good agreement with the 20.8 Å pore radius of the homologous residue of nAChR. In future work, we hope to optimize the spin labeling reaction to incorporate more than 2 spin labels per channel. This would afford us greater signal to noise in the time domain and would allow for a more robust interpretation of the distances.

The results show the applicability of SDSL and ESR for distance measurements in the glycine receptor. We show that the MTSSL can be incorporated M3 residues, which were thought to be relatively inaccessible in the lipid bilayer. We were able to label the channel reconstituted in lipid vesicles. Most membrane proteins have been spin labeled in detergent micelles,<sup>[28, 84, 94, 97]</sup> which increases the accessibility of the spin label to the residue of interest.

This is not an option for M3 residues of the glycine receptor, as these residues can only be labeled in the presence of agonist. State-dependent labeling is not feasible in detergent micelles, since the functionality of the channel may not be preserved in detergent as opposed to lipid vesicles.<sup>[117]</sup>

The data build on recent pulsed ESR research that measured distinct distances from multi-spin labeled light-harvesting chlorophyll *a/b* oligomers<sup>[97]</sup> or reaction intermediates in ribonucleotide reductase catalysis<sup>[67]</sup> to probe structural and mechanistic issues. With the experimental design illustrated in this paper, distinct distance constraints can be obtained on the homopentameric  $\alpha 1$  GlyR using ESR. Despite low signal to noise and incomplete labeling, we were able to observe multiple spin-spin interactions. Even though the spin labeled residue is putatively buried in the lipid bilayer, the residues were accessible to MTSSL. Thus ESR provides is well suited to measure distance constraints and determine subunit packings at the spin-labeled sites.

The presence of multi-spin interactions in ion-channels typically limits the use of CW-ESR methods for distance measurements. The limitation has elegantly been overcome in tetrameric KcsA channels by using sophisticated biochemistry to generate tandem dimers.<sup>[91]</sup> Although tandem dimers can be created for ligand gated ion-channels,<sup>[124]</sup> such as the GlyR, this adds another step of manipulation to the protein, and its extension to selectively labeling distinct subunits of overexpressed *pentameric* complexes is not direct.

Measurements of inter-subunit separations are likely to be a key determinant in developing a detailed understanding of triggered conformational motions in the GlyR. The cryo-EM image of nAChR<sup>[113]</sup> provides a good template for modeling the structure of the nicotinicoid receptors in their resting closed state. However, there exists limited structural information in

their open<sup>[107]</sup> and desensitized states.<sup>[125]</sup> Thus, the molecular mechanism of ligand gating is not well understood and is quite controversial. The proposed mechanisms involve the relative movements of entire segments of the proteins,<sup>[126]</sup> and hence the details may be resolved by the measurement of changes in inter-subunit packings in different allosteric states of the receptor. These DEER-ESR results, therefore, underscore future research that combine systematic nitroxide-scanning experiments on the GlyR with distance measurements, in the presence and absence of agonists, antagonists, and modulatory ligands in order to develop a detailed understanding of conformational changes that underlie the function of nicotinicoid receptors.

**Acknowledgement.** The research has been supported by an NIH NINDS grant (5R01NS53788-3) to SS, and by an NIDA grant (DA016381) to MC. We also gratefully acknowledge Darrin Lenhart, Emily Wickline, and Tommy Tillman for technical assistance in GlyR production.

## APPENDIX A

### GENERATION OF CYSTEINE MUTANTS OF THE GLYCINE RECEPTOR

The generation of new cysteine mutants of the glycine receptor is a multi-step process involving modification of the gene coding for the GlyR, incorporation of the GlyR gene into the baculoviral vector, amplification of the baculovirus, expression of mutant GlyR in *Spodoptera frugiperda* Sf9 insect cells, and purification and reconstitution of the mutant GlyR. Figure 1 shows an overview of the steps. This appendix will describe the methods used by the Saxena group in collaboration with the Cascio group, which are based on the work described by Cascio et al.<sup>[101]</sup>

The first step in creating a new cysteine mutant of the GlyR is to modify the gene. Our lab used the QuickChange® Site-Directed Mutagenesis Kit by Stratagene. Figure 2 summarizes the key steps for changing a single amino acid in the sequence using custom designed oligonucleotide primers, DNA polymerase, and a temperature cycler. Wild type glycine receptor contains three free cysteines, but we prepared a cys-null pFastBac plasmid where cysteines at positions 41, 290, and 345 have been replaced with serine, alanine, and serine respectively. This plasmid was used in the creation of all subsequent single cysteine mutations. Stratagene

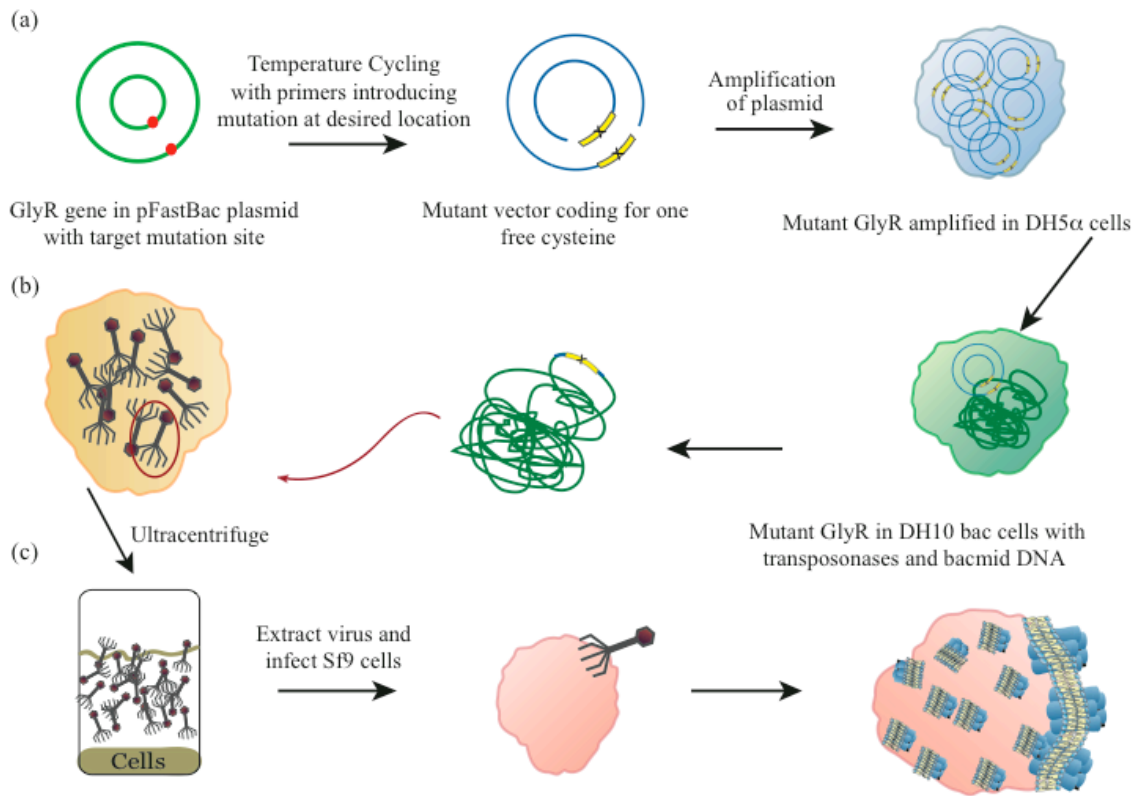


**Figure A. 1** Flow chart for creating mutant GlyR protein. a) The gene for GlyR is mutated to code for a single free cysteine at the desired location using site-directed mutagenesis. b) The mutant GlyR gene is incorporated into bacmid DNA, and virus is created and amplified. c) The baculovirus is used to infect Sf9 insect cells and overexpress mutant GlyR protein.

provides guidelines for designing the mutagenic oligonucleotide primers.<sup>[127]</sup> For every cysteine mutation, a forward and reverse primer was designed containing 25-45 bases with a melting temperature  $\geq 78^\circ\text{C}$  for optimal annealing. The melting temperature,  $T_m$  was estimated using the equation

$$T_m = 81.5 + 0.41(\%GC) - 675/N - \% \text{ mismatch} \quad [1]$$

where N is the number of bases in the primer, % GC is the percentage of G and C bases in the primer sequence, and % mismatch is the percentage of bases being changed. When designing the primer sequence, the mutation should be in the middle of the primer with 10-15 bases on either side. Also, a minimum of 40% of the bases should be either G or C, and both terminal ends of the primer should end in at least one G or C base. G-C base pairs form three hydrogen bonds, whereas A-T base pairs only form two. Therefore G-C base pairs contribute to a higher melting temperature. FPLC purified custom primers were purchased from Invitrogen.

Prior to all thermal cycling reactions, the concentration of the double stranded DNA template was quantified by measuring the UV absorbance at 260 nm. After subtracting the background signal at 350 nm from the absorbance at 260 nm, the concentration of DNA was calculated by

$$[\text{DNA}] = A(260) * \text{dilution factor} * 50 \text{ ng}/\mu\text{L} \quad [2]$$

The control and sample reaction conditions can be found in the QuickChange manual.<sup>[127]</sup> We have found 50 ng of double stranded DNA template to be an optimal concentration, but one can easily prepare multiple reactions with several concentrations. After thermal cycling, reaction products were stored at  $-20^\circ\text{C}$ . In order to digest the parental DNA, 1  $\mu\text{L}$  of the Dpn I restriction endonuclease was added to the sample and control reactions and incubated at  $37^\circ\text{C}$  for 1 hour. The digested DNA was stored at  $-20^\circ\text{C}$  until transformation of supercompetent cells.

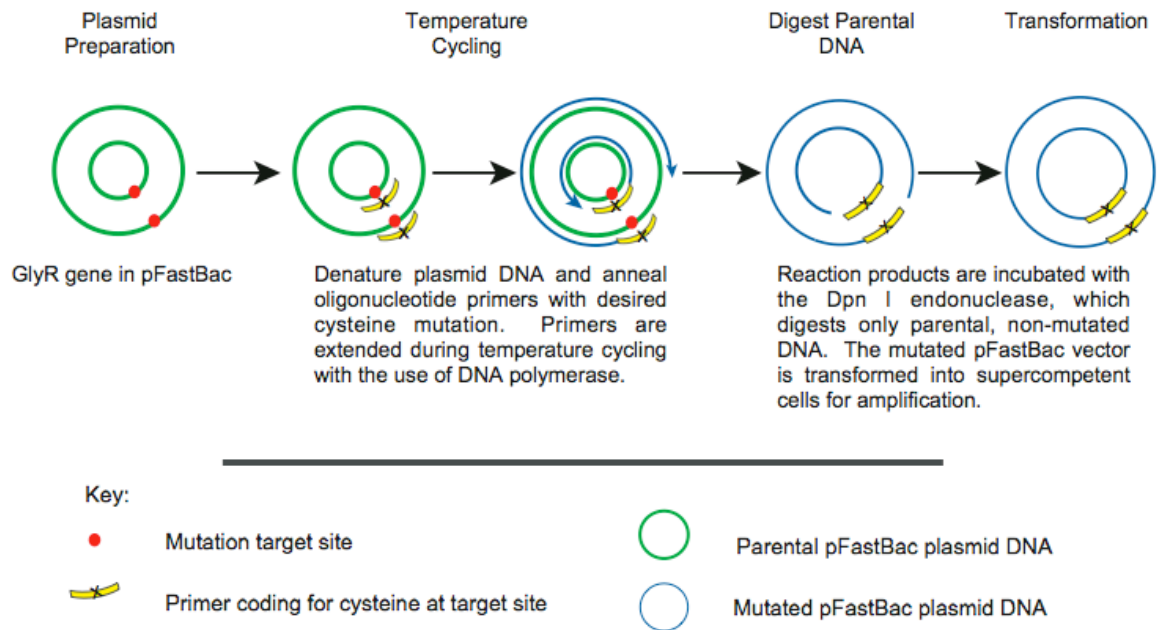


**Figure A. 2** Site-directed mutagenesis of the GlyR.

Prior to transformation, sterile NZY+ broth and LB-ampicillin agar plates were prepared. For color screening of the control experiment, LB-ampicillin agar plates containing X-gal and IPTG were prepared as well. The XL1-Blue supercompetent cells are very sensitive to temperature changes. Immediately upon receipt, they were stored at -80° C with minimal time out of dry ice. Failure to store correctly will result in a large loss of efficiency. After transformation of the thermal cycling reaction products, one may expect 10-1000 colonies. Well-isolated colonies were sterilely picked to media for plasmid purification by the Wizard® Minipreps DNA Purification System.<sup>[128]</sup> After purification, the concentration of the DNA was calculated as described above, and an aliquot was submitted for sequencing. The sequencing facility provides sample requirements (DNA and primer concentration, etc). Once the cysteine mutation in pFastBac was confirmed, a maxi prep was performed in order to generate sufficient quantities of DNA for permanent storage.

The Saxena and Cascio labs used the Bac-to-Bac® Baculovirus Expression System by Invitrogen<sup>[129]</sup> to incorporate the GlyR gene into Bacmid DNA, generate baculovirus, and infect insect cells for the overexpression of the GlyR. The purified mutant GlyR in pFastBac was used to transform DH10Bac *E. coli* cells (Fig. 1b). The DH10Bac transformation requires LB plates containing kanamycin, gentamicin, and tetracycline antibiotics, as well as Bluo-gal and IPTG for color screening. The Bac-to-Bac manual provides recipes for these solutions and media.<sup>[129]</sup> This transformation includes a color selection for phenotype selection. Colonies were restreaked to a fresh plate in order to confirm a white phenotype. After sterilely picking a white colony to media, the recombinant bacmid DNA could be isolated either using a commercially available mini prep or the protocol in Bac-to-Bac manual.<sup>[129]</sup> Invitrogen recommends using PCR to analyze the bacmid DNA and verify a successful transformation. The Saxena group has

attempted PCR and analysis by gel electrophoresis with the recommended primers on several occasions. *We consistently did not see the predicted PCR products on page 25 of the manual even in cases when the transformation was successful and the bacmid DNA was present.* It is difficult to verify a successful DH10bac transformation, but there are several options. One may perform PCR with the recommended primers and look for high molecular weight DNA on an agarose gel. Another option would be to simply transfect the insect cells with the isolated bacmid. If no bacmid is present, the transfection will be unsuccessful, and one may assume that the DH10bac transformation was also unsuccessful.

Once the bacmid DNA was isolated, it was used to transfect Sf9 insect cells and generate baculovirus (Fig. 1c). From this point on, Sf9 cells in log phase growth at >97% viability, a 27° C incubator, a laminar flow hood, and a microscope were required. After transfection, cells were visually inspected under the microscope for signs of viral infection. We observed signs of viral infection (granular appearance and detachment) 3-4 days post transfection, and harvested the P1 viral stock at this time. The baculovirus was amplified several times to generate a high titer stock. A viral plaque assay was performed to calculate the titer of the stock. An accurate titer aided in determining the appropriate volume of virus to use for routine infections to achieve the recommended multiplicity of infection. A western immunoblot was performed on a small infection of insect cells to verify that cells expressed the GlyR.

When the desired viral titer was reached and the expression of GlyR was verified, the baculovirus was sterilely stored and used for subsequent infections of insect cells. We typically infect between 800 mL and 1 L of cells at a density of  $1 \times 10^6$  cells/mL and a viability of >95% with a multiplicity of infection of ~5 viable virus particles per cell. Cells are harvested three days post infection by gentle centrifugation and stored at -20° C until purification.

The protocol for purifying and reconstituting functional GlyR (available in either the Saxena or Cascio lab) allows for the routine isolation of ~1 mg of purified GlyR for every 1 L of insect cells infected. Briefly, the Sf9 cells were harvested and lysed by probe tip sonication. The total particulate fraction was collected, salt-washed to remove peripheral proteins and solubilized in buffer containing 1% digitonin, 0.1% deoxycholate, and mixed phospholipids. The mixed micelles containing GlyR were affinity purified over 2-aminostrychnine-agarose. Next, the detergent was changed to 0.5% digitonin, 0.1% deoxycholate while the GlyR is bound, and then GlyR was eluted with glycine. Purified GlyR was reconstituted into small unilamellar lipid vesicles by dialysis against KPO<sub>4</sub> buffer and Bio-Beads (Bio-Rad). The reconstitution of the GlyR is non-trivial, as the protein strongly prefers to stay in detergent micelles. Effective reconstitution requires very large dialysis buffer volumes (5L), multiple buffer changes, and dialysis against Bio-Beads, which adsorb the cholate detergent molecules and allow the concentration of cholate in the dialysis cassette to go below the critical micelle concentration.<sup>[130]</sup> It is oftentimes still necessary to centrifuge the sample to pellet the reconstituted protein and repeat dialysis on the supernatant which can contain up to ~70% of the GlyR. Protein concentrations were determined by first performing a TCA precipitation followed by a modified Lowry using a standard bovine serum albumin sample to create a calibration curve.

During the generation of new cysteine mutants, aliquots were collected after each step of the purification (ie, whole cell lysate, cytosolic fraction, salt extract, detergent solubilized, etc) and a Western immunoblot was performed. A Western immunoblot can verify the presence of the GlyR as well as track the protein throughout the various stages of purification. It is not necessary to do a Western after every purification, but it is an excellent troubleshooting tool.

## **APPENDIX B**

### **SPIN LABELING CYSTEINES IN THE LIPID RECONSTITUTED GLYCINE RECEPTOR**

Site-directed spin labeling of membrane proteins requires careful consideration. The primary challenges include minimizing the non-specific association of the nitroxide spin label with the lipid head groups while simultaneously maximizing the accessibility and reactivity of the cysteines. This appendix addresses the challenges posed by the limited accessibility of transmembrane residues of GlyR to the nitroxide label due to the presence of the lipid bilayer. Several different strategies for spin labeling GlyR are discussed as well as the outcomes.

- **The use of reducing agents**

One of the simplest strategies used to increase the reactivity of cysteines is to ensure that they do not become oxidized during preparation using the strong reducing agent, dithiothreitol (DTT). When ~10 mM of DTT is added to solutions of GlyR, free cysteines are reduced, and cysteines engaged in a disulfide bridge are not disrupted. DTT should be removed immediately prior to spin labeling by gel filtration, dialysis, or a spin column.

- **Spin labeling reconstituted GlyR**

We achieved labeling of 1-2 cysteines per channel at the residues C286-C292 of the GlyR using the following protocol: After purification of each mutant, the protein was dialyzed in the presence of 1 mM DTT against 1-2 L of 25 mM potassium phosphate buffer to remove the salt from the sample solution and form lipid vesicles. Approximately 0.3 mL of lipids was added to each cassette after the first buffer change. In the last change of buffer, the protein was dialyzed against only potassium phosphate buffer to remove the DTT. After dialysis, the protein solutions were sonicated using a probe-tip sonicator to form unilamellar vesicles. The GlyR mutants were labeled in the presence of 0.030 M glycine. MTSSL was dissolved in acetonitrile and a 50 M excess over protein was added for 4 hours and again overnight. The reaction proceeded in the dark at 4 °C with shaking. Excess spin label was removed by dialysis against 2L of 25 mM potassium phosphate buffer overnight and again for 2 hours. Protein was collected by centrifugation at 65 krpm for 30 min. These samples provided enough spin labeled GlyR to give a DEER-ESR signal, but a modified Lowry indicated that a significant amount of protein failed to go into lipid vesicles in the reconstitution step. Since our signal is oftentimes dominated by the non-specific interaction of the label with the lipid, it is critical that we maximize the protein concentration of the ESR sample, and therefore the signal due to spin labeled cysteines.

- **Optimizing reconstitution of GlyR in lipid vesicles**

The detergent, digitonin, is used in the solubilization of the GlyR during its purification. While digitonin is an excellent detergent for retaining the structure and activity of the GlyR, it is very difficult to remove because of its very low critical micelle concentration (CMC) of <0.5 mM. The CMC describes the concentration above which a detergent will spontaneously form

micelles. A low CMC can be problematic during the reconstitution of a protein, like GlyR, because it is difficult to remove enough detergent molecules to disassociate the micelles. A common method for removing detergent and reconstituting protein into lipid vesicles is by dialysis. However, the protein must be dialyzed against a sufficiently large volume of buffer to create a large enough concentration gradient. Large dialysis volumes used with Bio-beads are an effective method for removing detergent, but it is very time intensive. As described in Chapter 3, protein is dialyzed against 4-5 L of buffer containing Bio-beads.<sup>[130]</sup> The buffer was changed every 24 hours for three days. After centrifugation, the supernatant was dialyzed again under the same conditions. This procedure improved our yield from 15% to >70% and was very reproducible.

- **Blocking the non-specific interaction of the spin label with the lipid head group**

We attempted to block the apparent electrostatic interaction of the nitroxide with the charged head groups of the lipid vesicles using a high salt solution. In a control experiment, we prepared a solution containing an equal concentration of lipids as our GlyR prep and identical spin labeling conditions. We added 1 M KCl to the solution, and allowed the reaction to proceed overnight. We passed the solution over a gel filtration column to remove excess spin label, and centrifuged as described above. Under these conditions, the high salt concentration did not appear to block the association of the MTSSL with the head groups, as indicated by CW ESR.

- **Spin labeling in detergent micelles**

Due to the difficulty of reconstituting the GlyR into the lipid bilayer and the non-specific interaction of the nitroxide spin label with the lipid head groups, we sought to spin label and perform our ESR measurement on GlyR in detergent micelles. The protein solution was concentrated down from ~8 mL to  $\leq 0.250$  mL using a 10K MWCO Amicon centrifuge filter and

passed over a G-50 sephadex gel filtration column to remove DTT prior to spin labeling. Detergent solubilized GlyR precipitated out at these low volumes. Therefore this method is not viable for our purposes because small volumes (~100  $\mu$ L) are needed for ESR spectroscopy.

- **Conclusions**

Although future work is needed to increase the number of spins per channel, we can summarize our findings. First, it is critical that care is taken to ensure that the protein is reconstituted into lipid vesicles. Gel filtration or dialysis without Bio-beads will not remove enough digitonin molecules to go below its CMC.<sup>[130]</sup> Next, DTT should be present through all steps of purification and should be removed immediately prior to spin labeling such that the reactive cysteines remain reduced. Also, adding a large excess of spin label (50-100 M over protein) two times appears to increase the concentration of cysteines that are modified. We may not be able to completely eliminate the interaction of the spin label with the lipids. However, if the concentration of both the spin labeled cysteines and the total GlyR in the ESR sample are increased, the non-specific signal should be minimized.

## BIBLIOGRAPHY

1. Hubbell, W., D. Cafiso, and C. Altenbach, *Identifying conformational changes with site-directed spin labeling*. Nat. Struc. Bio., 2000. **7**: p. 735-739.
2. Columbus, L. and W. Hubbell, *A new spin on protein dynamics*. Trends Biochem. Sci., 2002. **27**: p. 288-295.
3. Altenbach, C., T. Marti, H. Khorana, et al., *A method to determine transmembrane protein structure: Spin labeling of bacteriorhodopsin mutants*. Science, 1990. **248**: p. 1088.
4. Altenbach, C., S. Flitsch, H. Khorana, et al., *Structural studies on transmembrane proteins. 2. Spin labeling of bacteriorhodopsin mutants at unique cysteines*. Biochem., 1989. **28**: p. 7806-7812.
5. Cornish, V., D. Benson, C. Altenbach, et al., *Site-specific incorporation of biophysical probes into proteins*. Proc. Natl. Acad. Sci. USA, 1994. **91**: p. 2910-2914.
6. Hubbell, W., A. Gross, R. Langen, et al., *Recent advances in site-directed spin labeling of proteins*. Cur. Op. Struc. Bio., 1998. **8**: p. 649-656.
7. Farrens, D.L., C. Altenbach, K. Yang, et al., *Requirement of rigid-body motion of transmembrane helices for light activation of rhodopsin*. Science, 1996. **274**: p. 768-770.
8. Mchaourab, H.S., M. Lietzow, K. Hideg, et al., *Motion of spin-labeled side chains in T4 lysozyme. Correlation with protein structure and dynamics*. Biochem., 1996. **35**: p. 7692-7704.
9. Langen, R., K. Oh, D. Cascio, et al., *Crystal structures of spin labeled T4 lysozyme mutants: Implications for the interpretation of EPR spectra in terms of structure*. Biochem., 2000. **39**: p. 8396-8405.
10. Glasgow, B., O. Gasymov, A. Abduragimov, et al., *Side chain mobility and ligand interactions of the G strand of tear lipocalins by site-directed spin labeling*. Biochem., 1999. **38**: p. 13707-13716.
11. Altenbach, C., K. Oh, R. Trabanino, et al., *Estimation of inter-residue distances in spin labeled proteins at physiological temperatures: Experimental strategies and practical limitations*. Biochem., 2001. **40**: p. 15471-15482.

12. Gross, A., L. Columbus, K. Hideg, et al., *Structure of the KcsA potassium channel from Streptomyces lividans: A site-directed spin labeling study of the second transmembrane segment*. *Biochem.*, 1999. **38**: p. 10324-10335.
13. Gross, A. and W. Hubbell, *Identification of protein side chains near the membrane-aqueous interface: A site-directed spin labeling study of KcsA*. *Biochem.*, 2002. **41**: p. 1123-1128.
14. Langen, R., J. Isas, H. Luecke, et al., *Membrane-mediated assembly of annexins studied by site-directed spin labeling*. *J. Bio. Chem.*, 1998. **273**(35): p. 22453-22457.
15. Lin, Y., R. Nielsen, D. Murray, et al., *Docking phospholipase A2 on membranes using electrostatic potential-modulated spin relaxation magnetic resonance*. *Science*, 1998. **279**: p. 1925-1928.
16. Mchaorab, H., K. Oh, C. Fang, et al., *Conformation of T4 lysozyme in solution. Hinge-bending motion and the substrate-induced conformational transition studied by site-directed spin labeling*. *Biochem.*, 1997b. **36**: p. 307.
17. Mchaourab, H.S., M. Lietzow, K. Hideg, et al., *Motion of spin-labeled side chains in T4 lysozyme. Correlation with protein structure and dynamics*. *Biochem.*, 1996. **35**: p. 7692-7704.
18. Mollaaghababa, R., H. Steinhoff, W. Hubbell, et al., *Time-resolved site-directed spin-labeling studies of bacteriorhodopsin: Loop-specific conformational changes in M*. *Biochem.*, 2000. **39**: p. 1120-1127.
19. Qin, P., K. Hideg, J. Feigon, et al., *Monitoring RNA base structure and dynamics using site-directed spin labeling*. *Biochem.*, 2003. **42**: p. 6772-6783.
20. Shin, Y., C. Levinthal, F. Levinthal, et al., *Colicin E1 binding to membranes: Time-resolved studies of spin-labeled mutants*. *Science*, 1993. **259**: p. 960-963.
21. Voss, J., M. He, W. Hubbell, et al., *Site-directed spin labeling demonstrates that transmembrane domain XII in the lactose permease of escherichia coli is an  $\alpha$ -helix*. *Biochem.*, 1996. **35**: p. 12915-12918.
22. Voss, J., J. Wu, W. Hubbell, et al., *Helix packing in the lactose permease of escherichia coli: Distances between site-directed nitroxides and a lanthanide*. *Biochem.*, 2001. **40**: p. 3184-3188.
23. Yang, K., D. Farrens, C. Altenbach, et al., *Structure and function in rhodopsin. Cysteines65 and 316 are in proximity in a rhodopsin mutant as indicated by disulfide formation and interactions between attached spin labels*. *Biochem.*, 1996. **35**: p. 14040-14046.
24. Perozo, E., D. Cortes, and L. Cuello, *Structural rearrangements underlying K<sup>+</sup> channel activation gating*. *Science*, 1999. **285**: p. 73-78.

25. Liu, Y., P. Sompornpisut, and E. Perozo, *Structure of the KcsA channel intracellular gate in the open state*. *Nature Struc. Bio*, 2001. **8**: p. 883-887.
26. Cortes, D., L. Cuello, and E. Perozo, *Molecular architecture of full-length KcsA: Role of cytoplasmic domains in ion permeation and activation gating*. *J. Gen. Physiol.*, 2001. **117**(2): p. 165-180.
27. Li, J., Q. Xu, D. Cortes, et al., *Reactions of cysteines substituted in the amphipathic N-terminal tail of a bacterial potassium channel with hydrophilic and hydrophobic maleimides*. *Proc. Natl. Acad. Sci. USA*, 2002. **99**(18): p. 11605-11610.
28. Perozo, E., A. Kloda, D. Cortes, et al., *Site-directed spin-labeling analysis of reconstituted MscL in the closed state*. *J. Gen. Physiol.*, 2001. **118**: p. 193-205.
29. Perozo, E., *New structural perspectives on K<sup>+</sup> channel gating*. *Structure*, 2002. **10**: p. 1027-1029.
30. Perozo, E., D.M. Cortes, P. Sompornpisut, et al., *Open channel structure of MscL and the gating mechanism of mechanosensitive channels*. *Nature*, 2002. **418**(6901): p. 942-948.
31. Perozo, E., D. Cortes, P. Sompornpisut, et al., *Open channel structure of MscL and the gating mechanism of mechanosensitive channels*. *Nature*, 2002. **418**(8): p. 942.
32. Bezannilla, F. and E. Perozo, *Force and voltage sensors in one structure*. *Science*, 2002. **298**.
33. Eaton, S.S., K.M. Moore, B.M. Sawant, et al., *Use of the EPR half-field transition to determine the interspin distance and orientation of the interspin vector in systems of two unpaired electrons*. *J. Am. Chem. Soc.*, 1983. **105**: p. 6560.
34. Kurshev, V.V., A.M. Raitsimring, and Y.D. Tsvetkov, *Selection of the dipolar interaction by the "2+1" Pulse Train ESE*. *J. Magn. Reson.*, 1989. **81**(3): p. 441-454.
35. Rabenstein, M.D. and Y.K. Shin, *Determination of the distance between spin labels attached to a macromolecule*. *Proc. Natl. Acad. Sci.*, 1995. **92**: p. 8239.
36. Saxena, S. and J.H. Freed, *Theory of Double Quantum Two Dimensional Electron Spin Resonance with application to distance measurements*. *J. Chem Phys.*, 1997. **107**: p. 1317.
37. Milov, A.D., A.G. Maryasov, and Y.D. Tsvetkov, *Pulsed electron double resonance (PELDOR) and its applications in free-radicals research*. *Appl. Magn. Reson.*, 1998. **15**: p. 107-143.
38. Pannier, M., S. Veit, A. Godt, et al., *Dead-time free measurement of dipole-dipole interactions between electron spins*. *J. Mag Res*, 2000. **142**: p. 331.

39. Borbat, P.P., J.H. Davis, S.E. Butcher, et al., *Measurement of Large Distances in Biomolecules Using Double-Quantum Filtered Refocused Electron Spin-Echoes*. J. Am. Chem. Soc., 2004. **126**: p. 7746-7747.
40. Schiemann, O., N. Piton, Y. Mu, et al., *A PELDOR-based nanometer distance ruler for oligonucleotides*. J. Am. Chem. Soc., 2004. **126**: p. 5722-5729.
41. Bonora, M., J. Becker, and S. Saxena, *Suppression of electron spin-echo envelope modulation peaks in double quantum coherence electron spin resonance*. J. Magn. Reson., 2004. **170**: p. 278-283.
42. Banham, J., C. Timmel, R. Abbott, et al., *The characterization of weak protein-protein interactions: Evidence from DEER for the trimerization of a von Willebrand Factor A domain in solution*. Angew. Chem. Int. Ed., 2006. **45**: p. 1058-1061.
43. Pornsuwan, S., G. Bird, C. Schafmeister, et al., *Flexibility and lengths of bis-peptide nanostructures by electron spin resonance*. J. Am. Chem. Soc, 2006. **128**: p. 3876-3877.
44. Bode, B., D. Margraf, J. Plackmeyer, et al., *Counting the monomers in nanometer-sized oligomers by pulsed electron-electron double resonance*. J. Am. Chem. Soc, 2007. **129**: p. 6736-6745.
45. Pake, G.E., *Nuclear resonance absorption in hydrated crystals: Fine structure of the proton line*. J. Chem. Phys, 1948. **16**: p. 327-326.
46. Jeschke, G., *DeerAnalysis2006*. 2006: [www.mpip-mainz.mpg.de/~jeschke/distance.html](http://www.mpip-mainz.mpg.de/~jeschke/distance.html).
47. Chiang, Y.-W., P. Borbat, and J.H. Freed, *The determination of pair distance distributions by pulsed ESR using Tikhonov regularization*. J. Magn. Reson., 2005. **172**: p. 279.
48. Tikhonov, A. and V. Arsenin, *Solutions of ill-posed problems*. 1977, New York: Wiley.
49. Milov, A.D., Y.D. Tsvetkov, F. Formaggio, et al., *The secondary structure of a membrane-modifying peptide in a supramolecular assembly studied by PELDOR and CW-ESR spectroscopies*. J. Am. Chem. Soc., 2001. **123**: p. 3784-3789.
50. Milov, A.D., Y.D. Tsvetkov, F. Formaggio, et al., *Self-Assembling properties of membrane-modifying peptides studied by PELDOR and CW-ESR spectroscopies*. J. Am. Chem. Soc., 2000. **122**: p. 3843-3848.
51. Milov, A.D., A.B. Ponomarev, and Y.D. Tsvetkov, *Electron-electron double resonance in electron spin echo: model biradical systems and the sensitized photolysis of decalin*. Chem. Phys. Let., 1984. **110**: p. 67-72.
52. Lesser, D., M. Kurpiewski, and L. Jen-Jacobson, *The energetic basis of specificity in the EcoRI endonuclease-DNA interaction*. Science, 1990. **250**: p. 776-786.

53. Sapienza, P., C. dela Torre, W. McCoy, et al., *Thermodynamic and Kinetic Basis for the Relaxed DNA Sequence Specificity of "Promiscuous" Mutant EcoRI Endonucleases*. J. Mol. Bio., 2005. **348**: p. 307-324.
54. Jen-Jacobson, L., L. Engler, J. Ames, et al., *Thermodynamic Parameters of Specific and Nonspecific Protein-DNA Binding*. Supramolecular Chemistry, 2000. **12**: p. 143-160.
55. Sapienza, P., J. Rosenberg, and L. Jen-Jacobson, *Structural and thermodynamic basis for enhanced DNA binding by a promiscuous mutant EcoRI endonuclease*. Structure, 2007. **15**: p. 1368-1382.
56. Kurpiewski, M., L. Engler, L. Wozniak, et al., *Mechanism of coupling between DNA recognition specificity and catalysis in EcoRI endonuclease*. Structure, 2004. **12**: p. 1775-1788.
57. Grigorescu, A., M. Horvath, P. Wilkosz, et al., *Restriction Endonucleases*, ed. A. Pingoud. 2004: Springer-Verlag. 137-177.
58. Kim, Y., J. Grable, R. Love, et al., *Refinement of EcoRI endonuclease crystal structure: A revised protein chain tracing*. Science, 1990. **249**: p. 1307-1309.
59. Pingoud, A., M. Fuxreiter, V. Pingoud, et al., Cell. Mol. Life Sci., 2005. **62**: p. 685-707.
60. Wright, D., W. Jack, and P. Modrich, *The Kinetic Mechanism of EcoRI Endonuclease*. J. Bio. Chem., 1999. **274**: p. 31896-31902.
61. Berman, H., J. Westbrook, Z. Feng, et al., Nucleic Acids Res., 2000. **28**: p. 235.
62. Jen-Jacobson, L., M. Kurpiewski, D. Lesser, et al., *Coordinate ion pair formation between EcoRI endonuclease and DNA*. J. Biol. Chem., 1983. **258**: p. 14638-14646.
63. Siebenlist, U. and W. Gilbert, *Contacts between Escherichia coli RNA polymerase and an early promoter phage T7*. Proc. Natl. Acad. Sci. U. S. A., 1980. **77**: p. 122-126.
64. Martin, R.E., M. Pannier, F. Diederich, et al., *Determination of end-to-end distances in a series of TEMPO diradicals of up to 2.8 nm length with a new four-pulse double electron electron resonance experiment*. Angew. Chem. Intl. Ed., 1998. **37**: p. 2834-2837.
65. Hilger, D., Y. Polyhach, E. Padan, et al., *High-resolution structure of a Na<sup>+</sup>/H<sup>+</sup> antiporter dimer obtained by pulsed electron paramagnetic resonance distance measurements*. Biophys. J., 2007. **93**: p. 3675-3683.
66. Smirnova, I., V. Kasho, J.-Y. Choe, et al., *Sugar binding induces an outward facing conformation of LacY*. Proc Natl Acad Sci U S A, 2007. **104**: p. 16504-16509.
67. Bennati, M., J. Robblee, V. Mugnaini, et al., *EPR distance measurements support a model for long-range radical initiation in E. coli ribonucleotide reductase*. J. Am. Chem. Soc, 2005. **127**: p. 15014-15015.

68. Galiano, L., M. Bonora, and G. Fanucci, *Interflap distances in HIV-1 protease determined by pulsed EPR measurements*. J. Am. Chem. Soc., 2007. **129**: p. 11004-11005.
69. Milov, A., R.I. Samoilova, Y.D. Tsvetkov, et al., *Self-aggregation of spin-labeled alamethicin in ePC vesicles studied by pulsed electron-electron double resonance*. J. Am. Chem. Soc., 2007. **129**: p. 9260-9261.
70. Piton, N., Y. Mu, G. Stock, et al., *Base-specific spin labeling of RNA for structure determination*. Nucleic Acids Res., 2007. **35**: p. 3128-3143.
71. Godt, A., M. Schulte, H. Zimmermann, et al., *How flexible are poly(para-phenyleneethynylene)s?* Angew. Chem. Int. Ed., 2006. **45**: p. 7560-7564.
72. Sen, K.I., T. Logan, and P.G. Fajer, *Protein Dynamics and Monomer-Monomer Interactions in AntR Activation by Electron Paramagnetic Resonance and Double Electron-Electron Resonance*. Biochem., 2007. **46**: p. 11639-11649.
73. Jeschke, G., A. Koch, U. Jonas, et al., *Direct conversion of EPR dipolar time evolution data to distance distributions*. J. Magn. Reson., 2002. **155**: p. 72-82.
74. Jen-Jacobson, L., *Protein-DNA recognition complexes: Conservation of structure and binding energy in the transition state*. Biopolymers, 1997. **44**: p. 153-180.
75. Halford, S. and J. Marko, Nucleic Acids Res., 2004. **32**: p. 3040.
76. Terry, B., W. Jack, and P. Modrich, J. Biol. Chem., 1985. **260**: p. 13130-13137.
77. Altenbach, C., T. Marti, H.G. Khorana, et al., *Transmembrane protein structure: Spin labeling of bacteriorhodopsin mutants*. Science, 1990. **248**: p. 1088-1092.
78. Hubbell, W.L., A. Gross, R. Langen, et al., *Recent advances in site-directed spin labeling of proteins*. Cur. Op. Struct. Bio., 1998. **8**: p. 649-656.
79. Hubbell, W.L., D.S. Cafiso, and C. Altenbach, *Identifying conformational changes with site-directed spin labeling*. Nature Struct. Bio., 2000. **7**(9): p. 735-739.
80. Schneider, D.J. and J.H. Freed, *Spin Relaxation and Motional Dynamics*, in *Advances in Chemical Physics, Vol LXIII*, J. O. Hirschfelder, R. E. Wyatt, and R.D. Coalson., Editors. 1989, Wiley: New York.
81. Altenbach, C., D.A. Greenhalgh, H.G. Khorana, et al., *A collision gradient method to determine the immersion depth of nitroxides in lipid bilayer: Application to spin-labeled mutants of bacteriorhodopsin*. Proc. Nat. Acad. Sci., 1994. **91**: p. 1667.
82. Budil, D.E., S. Lee, S. Saxena, et al., *Nonlinear-least-squares analysis of slow-motion EPR spectra in one and two dimensions using a modified Levenberg-Marquardt Algorithm*. J. Magn. Reson. Series A, 1996. **120**: p. 155.

83. Cuello, L., D.M. Cortes, and E. Perozo, *Molecular Architecture of the KvAP Voltage-Dependent K<sup>+</sup> Channel in a Lipid Bilayer*. Science, 2004. **306**.
84. Lukasik, S., K. Ho, and D. Cafiso, *Molecular basis for substrate-dependent transmembrane signaling in an outer-membrane transporter*. J. Mol. Biol., 2007. **370**: p. 807-811.
85. Kim, M., G. Fanucci, and D. Cafiso, *Substrate-dependent transmembrane signaling in TonB-dependent transporters is not conserved*. Proc Natl Acad Sci U S A, 2007. **104**: p. 11975-11980.
86. Lu, X., Y. Zhang, and Y.-K. Shin, *Supramolecular SNARE assembly precedes hemifusion in SNARE-mediated membrane fusion*. Nat. Struct. Mol. Biol., 2008. **15**: p. 700-706.
87. Hilger, D., Y. Polyhach, G. Jung, et al., *Backbone structure of transmembrane domain IX of the Na<sup>+</sup>/Proline transporter PutP of Escherichia coli*. Biophys. J., 2009. **96**: p. 217-225.
88. Borbat, P., K. Surendhran, M. Bortolus, et al., *Conformational motion of the ABC transporter MsbA induced by ATP hydrolysis*. PLoS Biology, 2007. **5**: p. 2211-2219.
89. Dzikovski, B., P. Borbat, and J. Freed, *Spin-Labeled Gramicidin A: Channel Formation and Dissociation*. Biophys. J., 2004. **87**: p. 3504-3517.
90. Perozo, E., D.M. Cortes, and L. Cuello, *Structural rearrangements underlying K<sup>+</sup> channel activation gating*. Science, 1999. **285**: p. 73.
91. Liu, Y.-S., P. Sompornpisut, and E. Perozo, *Structure of the KcsA channel intracellular gate in the open state*. Nature Struct. Bio., 2001. **8**(10): p. 883-887.
92. Perozo, E., *New structural perspectives on K<sup>+</sup> channel gating*. Structure, 2002. **10**: p. 1027.
93. Perozo, E., D.M. Cortes, P. Sompornpisut, et al., *Open channel structure of MscL and the gating mechanism of mechanosensitive channels*. Nature, 2002. **418**: p. 942.
94. Vamvouka, M., J. Cieslak, N. Van Eps, et al., *The structure of the lipid-embedded potassium channel voltage sensor determined by double electron-electron resonance spectroscopy*. Protein Sci., 2008. **17**: p. 506-517.
95. Chakrapani, S., L. Cuello, D.M. Cortes, et al., *Structural dynamics of an isolated voltage-sensor domain in a lipid bilayer*. Structure, 2008. **16**: p. 398-409.
96. Hilger, D., H. Jung, E. Padan, et al., *Assessing Oligomerization of Membrane Proteins by Four-Pulse DEER: pH-Dependent Dimerization of NhaA Na<sup>+</sup>/H<sup>+</sup> Antiporter of E. coli*. Biophys. J., 2005. **89**: p. 1328-1338.

97. Jeschke, G., A. Bender, T. Schweikardt, et al., *Localization of the N-terminal Domain in Light-harvesting Chlorophyll a/b Protein by EPR Measurements*. J. Bio. Chem., 2005. **280**(19): p. 18623-18630.
98. Sicoli, G., *Double electron-electron resonance (DEER): A convenient method to probe DNA conformational changes*. Angew. Chem. Int. Ed., 2008. **47**: p. 735-737.
99. Ward, R., D. Keeble, H. El-Mkami, et al., *Distance determination in heterogeneous DNA model systems by pulsed EPR*. ChemBioChem, 2007. **8**: p. 1957-1960.
100. Milov, A.D., A.G. Maryasov, Y.D. Tsvetkov, et al., *Pulsed ELDOR in spin-labeled polypeptides*. Chem. Phys. Lett., 1999. **303**: p. 135-143.
101. Cascio, M., N. Schoppa, R. Grodzicki, et al., *Functional expression and purification of a homomeric human  $\alpha 1$  glycine receptor in baculovirus-infected insect cells*. J. Bio. Chem., 1993. **268**(29): p. 22135-22142.
102. Cascio, M., S. Shenkel, R. Grodzicki, et al., *Functional reconstitution and characterization of recombinant human  $\alpha 1$ -glycine receptors*. J. Bio. Chem., 2001. **276**(24): p. 20981-20988.
103. Karim, C., J. Stamm, J. Karim, et al., *Cysteine reactivity and oligomeric structures of phospholamban and its mutants*. Biochem., 1998. **37**: p. 12074-12081.
104. Akabas, M.H., C. Kaufmann, P. Archdeacon, et al., *Identification of acetylcholine receptor channel-lining residues in the entire M2 segment of the  $\alpha$  subunit*. Neuron, 1994. **13**: p. 919-927.
105. Cascio, M., *Structure and function of the glycine receptor and related nicotinicoid receptors*. J. Bio. Chem., 2004. **279**: p. 19383.
106. Lynch, J., *Molecular structure and function of the glycine receptor chloride channel*. Physiol. Rev, 2004. **84**: p. 1051.
107. Unwin, N., *Acetylcholine receptor channel imaged in the open state*. Nature, 1995. **373**: p. 6509.
108. Miyazawa, A., Y. Fujiyoshi, and N. Unwin, *Nicotinic Acetylcholine receptor at 4.6 Å resolution: Transverse tunnels in the channel wall*. J. Mol. Bio., 1999. **288**: p. 765.
109. Miyazawa, A., Y. Fujiyoshi, and N. Unwin, *Structure and gating mechanism of the acetylcholine receptor pore*. Nature, 2003. **423**: p. 949-955.
110. Nayeem, N., T. Green, I. Martin, et al., *Quaternary structure of the native GABA<sub>A</sub> receptor determined by electron microscopy image analysis*. J. Neurochem, 1994. **62**: p. 815.

111. Brejc, K., W. van Dijk, R. Klaassen, et al., *Crystal structure of an ACh-binding protein reveals the ligand-binding domain of nicotinic receptors*. Nature, 2001. **411**: p. 269.
112. Grutter, T., L. de Carvalho, V. Dufresne, et al., *Molecular tuning of fast gating in pentameric ligand-gated ion channels*. Proc Natl Acad Sci U S A, 2005. **102**: p. 18207-18212.
113. Unwin, N., *Refined Structure of the Nicotinic Acetylcholine Receptor at 4 Angstroms Resolution*. J. Mol. Biol., 2005. **346**: p. 967-989.
114. Hilf, R. and R. Dutzler, *X-ray structure of a prokaryotic pentameric ligand-gated ion channel*. Nature, 2008. **452**: p. 375-379.
115. Laube, B., G. Maksay, R. Schemm, et al., *Modulation of glycine receptor function: A novel approach for therapeutic intervention at inhibitory synapses?* Trends in Pharm. Sci., 2002. **23**(11): p. 519.
116. Wilson, G.G. and A. Karlin, *Acetylcholine Receptor Channel Structure in the Resting, Open, and Desensitized States Probed with the Substituted-Cysteine-Accessibility Method*. Proc. Natl. Acad. Sci. USA, 2001. **98**: p. 1241-1248.
117. Clarke, R., S. Goode, J. Johnson, et al., *Unpublished observation*.
118. Jenkins, A., E.P. Greenblatt, H.J. Faulkner, et al., *Evidence for a Common Binding Cavity for Three General Anesthetics within the GABAA Receptor*. J. Neurosci., 2001. **21**: p. RC136(1-4).
119. Kash, T.L., A. Jenkins, J.C. Kelley, et al., *Coupling of agonist binding to channel gating in the GABA(A) receptor*. Nature, 2003. **421**(6920): p. 272-5.
120. Jansen, M. and M.H. Akabas, *State-dependent cross-linking of the M2 and M3 segments: functional basis for the alignment of GABAA and acetylcholine receptor M3 segments*. J. Neurosci., 2006. **26**: p. 4492-4499.
121. Lobo, I., M. Mascia, J. Trudell, et al., *Channel gating of glycine receptor changes accessibility to residues implicated in receptor potentiation by alcohols and anesthetics*. J. Biol. Chem., 2004. **279**: p. 33919-33927.
122. Lobo, I., J. Trudell, and R. Harris, *Cross-linking of glycine receptor transmembrane segments two and three alters coupling of ligand binding with channel opening*. J. Neurochem., 2004. **90**: p. 962-969.
123. Williams, D.B. and M.H. Akabas, *g-Aminobutyric Acid increases the Water Accessibility of M3 Membrane-spanning Segment Residues in g-Aminobutyric Acid Type A Receptors*. Biophys. J., 1999. **77**: p. 2563-2574.
124. Grudzinska, J., R. Schemm, S. Haeger, et al., *The beta subunit determines the ligand binding properties of synaptic glycine receptors*. Neuron, 2005. **45**(5): p. 727-739.

125. Unwin, N., C. Toyoshima, and E. Kubalek, *Arrangement of the acetylcholine receptor subunits in the resting and desensitized states, determined by cryoelectron microscopy of crystallized Torpedo postsynaptic membranes*. J. Cell. Biol., 1988. **107**: p. 1123.
126. Karlin, A., *Emerging Structure of the Nicotinic Acetylcholine Receptors*. Nature Rev. Neurosci., 2002. **3**: p. 102.
127. Strategene, *Instruction Manual: Quickchange Site-directed mutagenesis kit*. 2002.
128. Promega, *Technical Bulletin*. Wizard Minipreps DNA Purification System, 2005.
129. Invitrogen, *Bac-to-Bac Baculovirus Expression System*. 2004.
130. Ruthstein, S., *Unpublished observation*. 2008.